

# The Vibrational Spectroscopy of Metal Carbonyls for Bio-Imaging and -Sensing

Received 00th January 20xx,  
Accepted 00th January 20xx

DOI: 10.1039/x0xx00000x

www.rsc.org/

Zhiyong Lam,<sup>a,b</sup> Kien Voon Kong,<sup>c</sup> Malini Olivo,<sup>b,d</sup> and Weng Kee Leong<sup>a</sup>

Transition metal carbonyls exhibit strong CO absorptions in the 2200–1800  $\text{cm}^{-1}$  region, which is free of interference from other functional groups. This feature has led to their applications in bio-imaging and -sensing, in particular through mid-IR, Raman and more recently, surface-enhanced Raman spectroscopy (SERS). Their use in mid-IR quantitative sensing based on vibrational intensities, and chemical sensing based on frequency shifts and vibrational lifetimes, is reviewed. Their development for Raman sensing following the breakthrough in SERS highlights the potential of coupling metal carbonyls to plasmonic nanostructures as novel optical materials for SERS-based bio-imaging and -sensing.

## 1. Scope

Organometallic chemistry – the study of compounds with metal-carbon bond(s) – lies at the intersection between organic and inorganic chemistry. Early interests were fueled by its relevance to catalysis and its industrial applications. The Monsanto and Cativa catalyst systems for the manufacture of acetic acid, and Ziegler-Natta catalyst for the synthesis of polymers, are some examples.<sup>1–3</sup> Conventional wisdom built up from research in the field was that organometallic compounds were mainly air- and moisture-sensitive and for that reason, their relevance to the biological sciences was largely overlooked. The term “bioorganometallics” was introduced by Jaouen in 1985,<sup>4, 5</sup> and interests began to surge after the first International Symposium on Bioorganometallic Chemistry (ISBOMC) held in 2002. Current research interest is wide-ranging and includes applications in pharmaceuticals, bioassays and bioimaging.

One class of organometallic compounds which has found wide application in biology is the transition metal carbonyl complexes, i.e., complexes with carbon monoxide (CO) ligand(s) coordinated to the metal center. The first example,  $\text{Ni}(\text{CO})_4$ , was discovered by Ludwig Mond in 1890, and led subsequently to the Mond process, which uses its formation from CO gas as a means to purify and extract nickel from its ores.<sup>6</sup> CO is an unsaturated molecule due to the multiple (triple)  $\text{C}\equiv\text{O}$  bond. The interaction between CO and a metal centre involves the donation of a lone pair of electrons from

the carbon atom to the metal, and back donation from the metal to an anti-bonding orbital of the C-O bond (figure 1a). The extent of  $\pi$ -back donation is usually the main factor affecting the C-O bond order, and hence, the vibrational frequency. Bonding to a metal centre generally leads to a reduction in the C-O bond order, and the various bonding modes that a CO ligand can adopt, ranging from triply-bridging to terminal, leads to characteristic vibrational frequencies in various sub-regions of the 1650–2200  $\text{cm}^{-1}$  range.

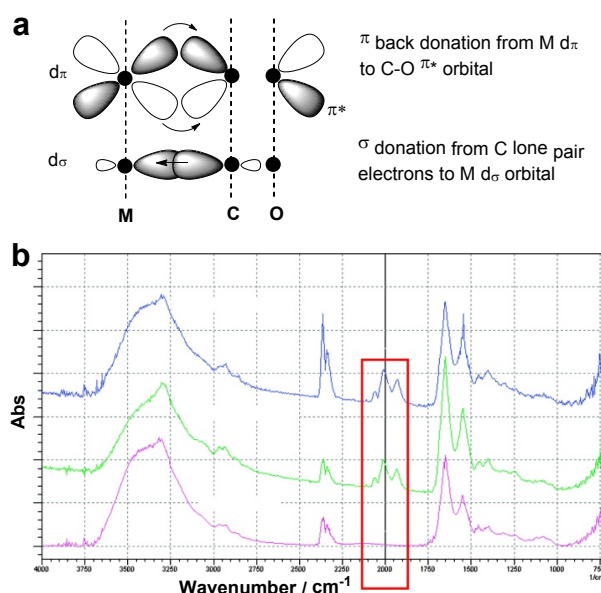


**Figure 1.** a) Orbital diagram showing the bonding between carbon monoxide with a transition metal centre. b) IR spectra recorded in absorbance mode of untreated mucosa cells (bottom), cells treated with a triosmium carbonyl cluster (middle and top). Boxed region shows carbonyl (CO) stretching vibrations of the organometallic fragment. Adapted from ref. 7 with permission from the American Chemical Society.

<sup>a</sup> Division of Chemistry and Biological Chemistry, Nanyang Technological University, Singapore.

<sup>b</sup> Singapore Bioimaging Consortium, Agency for Science, Technology and Research (A\*STAR), Singapore.

<sup>c</sup> Department of Chemistry, National Taiwan University, Taiwan.

<sup>d</sup> School of Physics, National University of Ireland, Galway, Ireland.

See DOI: 10.1039/x0xx00000x

This frequency range is relatively free from interference by other functional groups, and it is this property that drives the biological applications of metal carbonyls (figure 1b). The CO vibrational frequency can be tuned through changes in the ligand sphere, or through the charge on the complex (cationic or anionic species), to adjust the extent of  $\pi$ -back donation. This has allowed the development of responsive metal carbonyl bioprobes, which will be discussed later.

A number of reviews on various aspects of bioorganometallic chemistry, with chapters and sections on metal carbonyls, are available,<sup>8-14</sup> including some which are based on vibrational imaging.<sup>13, 14</sup> In contrast, the limelight in the current review is cast on the vibrational spectroscopy of metal carbonyls based on their vibrational properties, viz. intensity, frequency and lifetime. The manner in which different aspects of the vibrational spectroscopy of metal carbonyls have given rise to applications in bio-sensing and – imaging, from mid-IR to Raman, including surface-enhanced Raman spectroscopy (SERS), will be discussed.

## 2. Applications of mid-IR spectroscopy

### 2.1 Metal carbonyls as mid-IR probes

#### 2.1.1 Steroidal hormonal receptor assay

The earliest report on the use of metal carbonyls for mid-IR sensing was from the group of Jaouen.<sup>5, 15</sup> The study of steroid hormonal receptors in cancer cells, especially breast

carcinoma, was of interest and the available detection method then was based on radiolabelled hormones, which involved high cost and health hazards. Jaouen and co-workers realized the use of metal carbonyls as an alternative through a  $\eta^6$ -Cr(CO)<sub>3</sub> bound estradiol derivative, **1**, which binds onto estrogen receptors in lamb uterus cytosol.<sup>5, 15</sup> The complexation of Cr(CO)<sub>3</sub> yielded two stereoisomers, of which the  $\alpha$ -Cr(CO)<sub>3</sub> derivative showed stronger binding affinity. The precipitated protein from the lamb uterine cytosol, incubated with  $\alpha$ -**1**, was quantified by FT-IR spectroscopy.

Subsequently, estradiol with a alkyne functionality at the C17 $\alpha$ - position was complexed with small metal carbonyl clusters like [Co<sub>2</sub>(CO)<sub>6</sub>], [CpMo(CO)<sub>2</sub>]<sub>2</sub> and [Os<sub>3</sub>(CO)<sub>10</sub>] to form **2-4**, respectively.<sup>16, 17</sup> The complexation at the 17 $\alpha$ - position was well-tolerated with the metal cluster. However, relative binding affinity (RBA) was reduced with the bulkier triosmium cluster. Derivatization at the 2-, 4- and 16 $\alpha$ -positions with [Co<sub>2</sub>(CO)<sub>6</sub>] were also attempted, with the 4- and 16-derivatives binding estradiol receptors with reasonable affinity.<sup>17</sup>

The concept was extended to another oestrogen receptor binding molecule, hexestrol, which exhibited a higher binding affinity than estradiol; the Cr(CO)<sub>3</sub>-hexestrol derivative **5** had a relative binding affinity of 2%, making it suitable for labelling the semi-purified protein.<sup>18</sup> It was also extended to progesterone and glucocorticoid receptor assays; Cr(CO)<sub>3</sub>-, [Co<sub>2</sub>(CO)<sub>6</sub>]- and [CpMo(CO)<sub>2</sub>]<sub>2</sub>-mifepristone conjugates **6-8** showed binding affinity for cytosol progesterone and glucocorticoid receptors.<sup>19</sup>

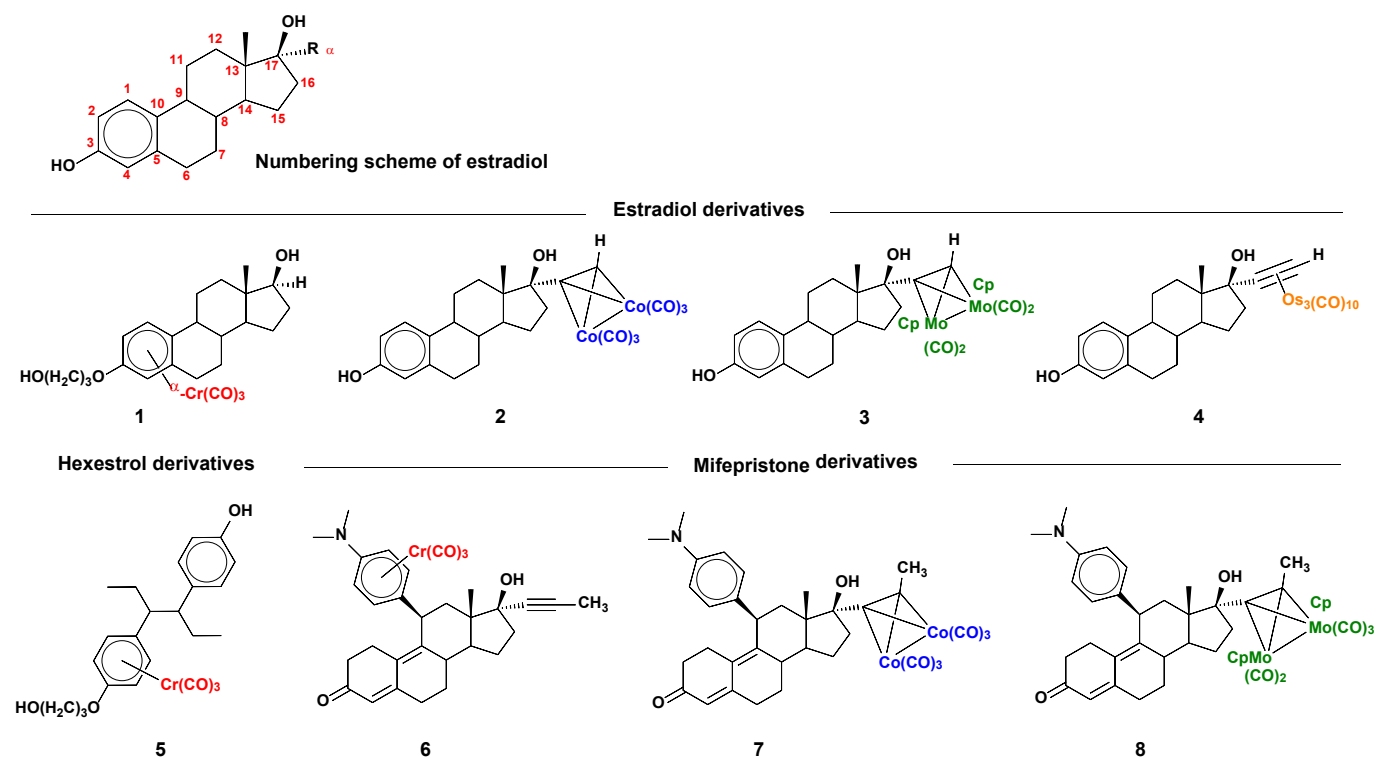


Figure 2. Molecular structures of metal carbonyl-steroid derivatives used for steroidal hormonal assay.

### 2.1.2 Carbonylmetalimmunoassay (CMIA)

The development of steroid hormone receptor assay led subsequently to a quantitative assay, termed carbonylmetalimmunoassay (CMIA). This new, non-radioisotopic immunoassay utilized transition metal carbonyl labelled analytes for FT-IR spectroscopic detection down to femtomolar concentrations.<sup>20</sup> The analyte to be detected was first conjugated to a stable organometallic carbonyl fragment (the tracer). In this competition-type immunoassay, a known amount of the tracer was incubated with the antibodies (the binding proteins) and unknown amounts of the analyte (to be detected). The analyte and tracer compete for binding to the limited amount of antibody. The unbound tracer was then extracted with organic solvents and quantified by FT-IR spectroscopy, thus allowing indirect determination of the amount of the analyte present (figure 3). This assay has been employed for the detection of anti-epileptic drugs like phenobarbital, carbamazepine, diphenylhydantoin, the anti-depressant nortriptyline and cortisol, with the use of the corresponding metal carbonyl conjugates **9-13** as tracers (figure 4).<sup>20-24</sup>

The CMIA concept was also extended to environmental sensing, with the detection of herbicides chlortoluron and atrazine. Anti-chlortoluron, -atrazine and -simazine (a derivative of atrazine) antibodies were generated and used in conjunction with the metal carbonyl derivatives **14-15** as tracers.<sup>25, 26</sup>

The simultaneous detection of two or more targets, also known as multiplex detection, can be incorporated into CMIA. FT-IR spectroscopy is ideal for multiplex detection owing to the narrow bandwidths of the molecular vibrational frequencies, which is advantageous for achieving minimal or non-overlapping of signals. Duplex and triplex detection of anti-epileptic drugs like carbamazepine, phenobarbital and diphenylhydantoin were demonstrated, using a different metal carbonyl for each target.<sup>27, 28</sup>

The sensing platform for CMIA has also been improved over the years. One such is solid-phase CMIA, which improved on the purification through immobilization of the capture agents. Using the strong interaction between biotin and streptavidin, poly-L-lysine and fourth generation Starburst dendrimers were functionalized with biotin and metal carbonyls, and shown to have good binding affinity towards streptavidin-coated microtiter plates.<sup>29</sup> A similar approach was adopted for metal carbonyl-dendrimer-antibody conjugates; antigens were spotted onto a nitrocellulose membrane, followed by addition of the conjugates as a label for selective detection.<sup>30, 31</sup> Use of the gold surface as an anchoring site was achieved using the strong Au-S interaction to immobilize biotin onto the gold surface. Avidin-metal carbonyl conjugates were able to bind to biotin on the gold surface and, in turn, biotin-metal carbonyl conjugates could bind to the avidin conjugate which was then detected by Fourier transform infrared reflection absorption spectroscopy (FT-IRRAS).<sup>32, 33</sup> Poly-L-lysine functionalized metal carbonyl was also shown to interact with a carboxylate functionalized gold surface via electrostatic interaction between the amine and carboxylate groups.<sup>34</sup>

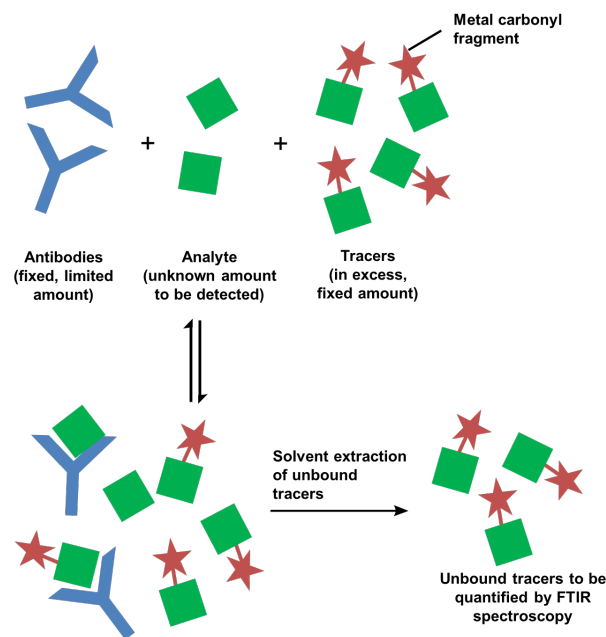


Figure 3. Schematic representation on the working principles of CMIA.

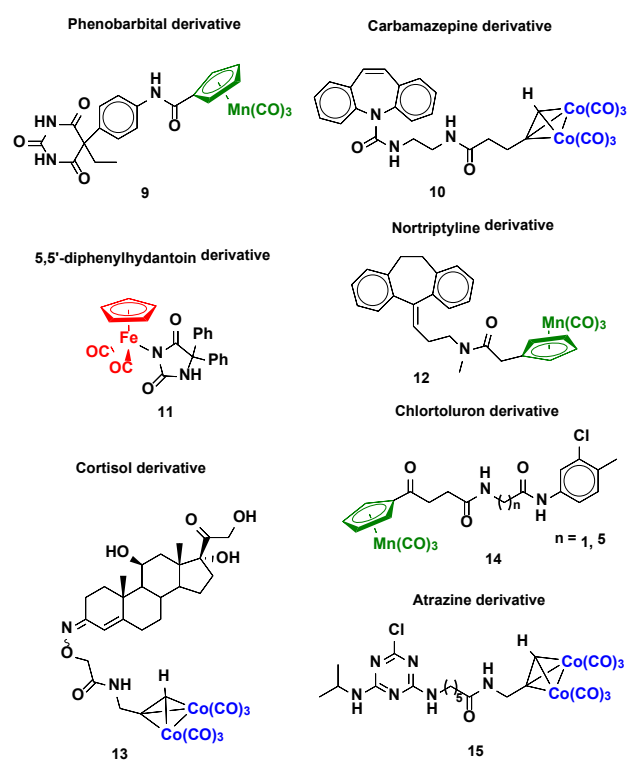


Figure 4. Metal carbonyl derivatives used as tracers in CMIA.

The disulfide-linked metal carbonyl, **16**, can be anchored onto gold nanoparticles and surface-enhanced infrared absorption (SEIRA) was observed (figure 5a).<sup>35</sup> This conjugate was further functionalized with antibodies, using carbodiimide coupling chemistry, and utilized as a secondary label to detect a mouse monoclonal anti-staphylococcal enterotoxin A (SEA)

antibody chemisorbed onto a planar gold surface.<sup>36</sup> The detection was via polarization modulation infrared reflection-absorption spectroscopy (PM-IRAAS) and atomic force microscopy (AFM).<sup>36</sup> Recently,  $\text{CpFe}(\text{CO})_2(\text{N-maleimidato})$ , **17**, was grafted onto thiol or amine-functionalized magnetic nanoparticles (MNP), followed by conjugation to antibodies (figure 5b).<sup>37</sup>

These approaches that utilized nanoparticles can be a means to amplify the CO signal as the metal carbonyl-ligand ratio can be varied, and they provide easy modification of the support without the need to functionalize the metal carbonyl directly.

### 2.1.3 IR probes for cellular imaging

The first example of mid-IR imaging of cells using a metal carbonyl was reported by Leong, *et al.*, with the stable and water-soluble triosmium carbonyl cluster,  $[\text{Os}_3(\text{CO})_{10}(\mu\text{-H})(\mu\text{-S}(\text{CH}_2)_{10}\text{COO})]\text{Na}$ , **18**, essentially an inorganic salt of a fatty acid conjugated to a metal carbonyl cluster, and its phosphatidylcholine analogue, **19**, as the probe (figure 6).<sup>7</sup> Chemical mapping in oral mucosa cells was carried out with an IR microscope fitted with a 64 x 64 pixel image plate detector. The chemical mapping at 2013  $\text{cm}^{-1}$  which corresponded to one of the CO vibration bands of the cluster correlated well to

the optical image, indicating internalization of the compound into the cells.

A growing interest in the transition metal carbonyls is in their potential as CO-releasing molecules (CORMs), i.e., complexes which can act as carriers for carbon monoxide, for delivery into biological systems for therapeutic purposes.<sup>38, 39</sup> The release of CO can be triggered in various ways, including the use of light; the term "photoCORMs" is used to describe such complexes.<sup>40, 41</sup> Zobi and Quaroni, *et al.*, reported the synthesis of a manganese photoCORM conjugated to the 5'-OH of the ribose sugar of vitamin B<sub>12</sub>, **20**, and its delivery into live 3T3 fibroblasts.<sup>42</sup> The uptake and cellular distribution of the B<sub>12</sub>-MnCORM was monitored by synchrotron FTIR spectromicroscopy in the live cells (figure 7a). The moderate spatial resolution only allowed the nucleus and cytoplasm to be distinguished. Although the uneven topography of the cells made quantification of the compound in the cells difficult, it was deduced that the compound accumulated in the nucleus, and this was supported by atomic absorption spectrophotometric measurements of the cell fractions.

Another growing interest is the development of multimodal imaging probes for correlative and more accurate detection. As an example, the rhenium tris-carbonyl derivatives **21-23**, which display IR and luminescent properties,

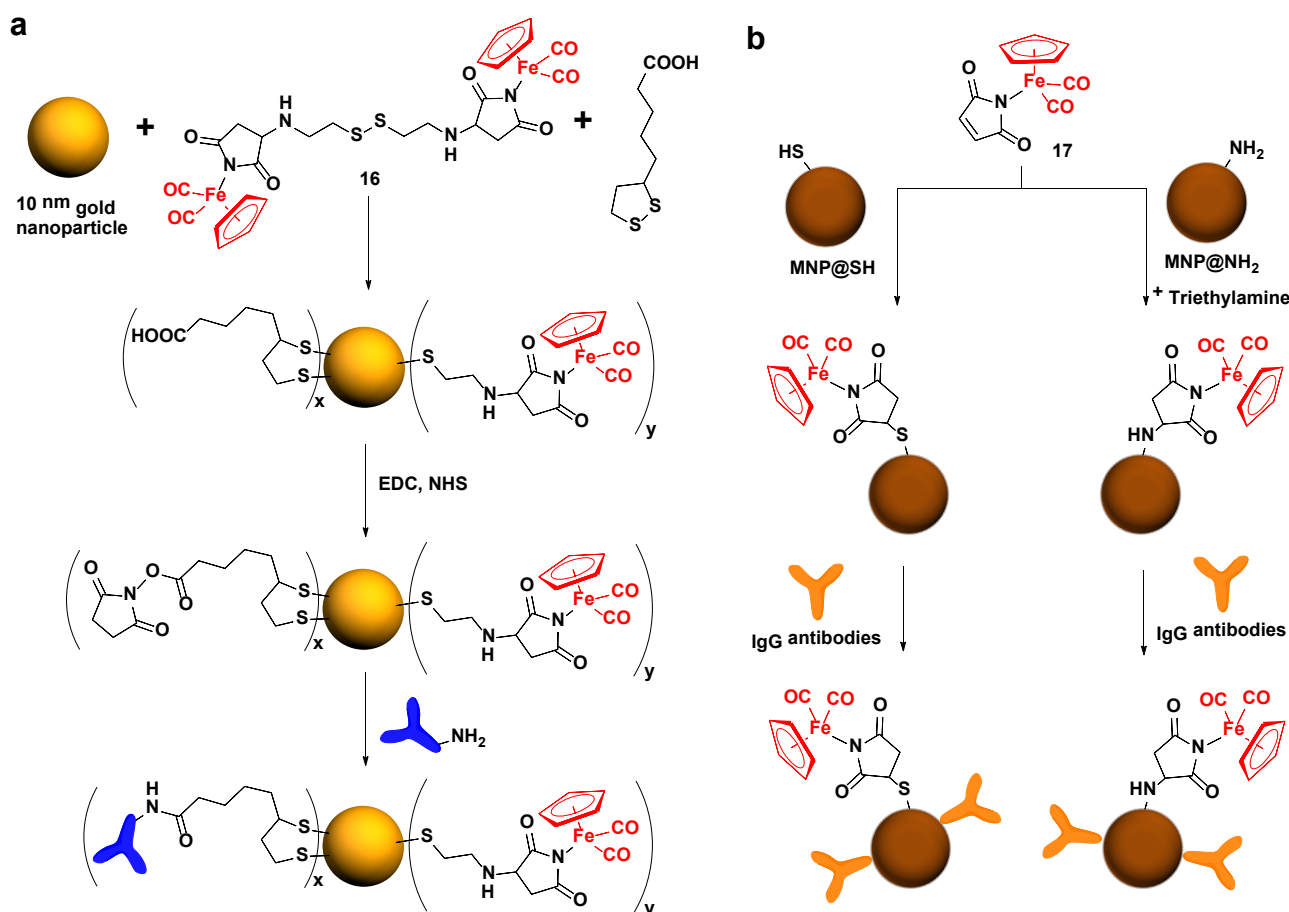


**Figure 5.** a) Synthesis of **16**-gold nanoparticle conjugates and immobilization of goat anti-mouse IgG antibody. Adapted from ref. 35 with permission from Elsevier. b) Synthesis of **17**-MNP conjugates and immobilization of IgG antibody. Adapted from ref. 36 with permission from Elsevier.

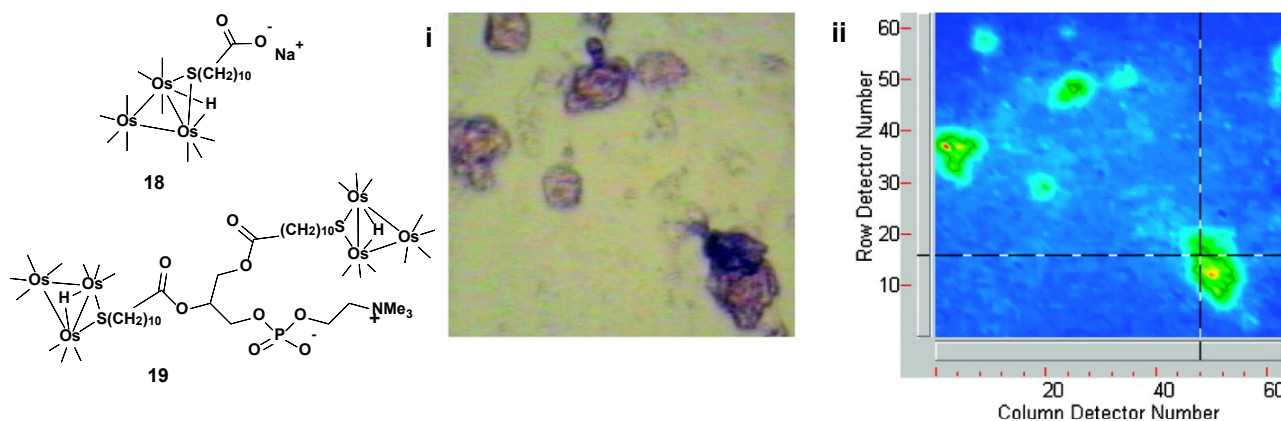


**Figure 6.** a) Molecular structure of  $[\text{Os}_3(\text{CO})_{10}(\mu\text{-H})(\mu\text{-S}(\text{CH}_2)_{10}\text{COO})]\text{Na}$ , **18**, and phosphatidylcholine analogue, **19**. The short lines extending from Os represent CO ligands. (i) Normal optical image and (ii) false-color IR image of oral mucosa cells treated with **18** ( $32\ \mu\text{M}$ ), taken at  $2013\ \text{cm}^{-1}$ , one of the carbonyl vibration band. Adapted from ref. 7 with permission from the American Chemical Society.

were utilized as single-core, multimodal probes for imaging breast cancer cells (figure 7b).<sup>43–45</sup> Synchrotron wide-field infrared spectromicroscopy of cells incubated with **21** was optimized with spatial oversampling, spectral pre-processing and deconvolution, to produce high definition FT-IR chemical images (figure 7c).<sup>43</sup> To further understand the localization of such complexes within the cells, correlative studies on the rhenium tris-carbonyl-mestranol conjugate **22** with a series of luminescent and vibrational imaging techniques (AFM-IR, synchrotron FT-IT microspectroscopy, synchrotron-based multiple beam FT-IR imaging, and confocal Raman microspectroscopy) were used to determine the presence of the complex in the Golgi apparatus.<sup>44</sup> Similarly, the  $[\text{CpRe}(\text{CO})_3]$ -hydroxytamoxifen conjugate **24** was utilized as an IR probe for synchrotron radiation FT-IR imaging in MDA-MB-231 cells. The localization of **24** in the nucleus was correlated with fluorescence images of DAPI-stained nucleus of the same cells.<sup>46</sup>

Though the multimodal probes mentioned above can facilitate correlation studies between fluorescence and IR imaging, the latter technique remains the more reliable for the quantification of cellular uptake.<sup>45</sup> This is because the quantum yield of a fluorescent probe is highly dependent on the environment, including the temperature and solvent,<sup>45, 47</sup> and is also highly susceptible to degradation through photobleaching and quenching. On the other hand, IR signals tend to be more stable and easily quantified via a calibration curve. Although the probe environment can induce broadening and/or a shift in the IR frequencies, peak areas remain relatively constant and hence reliable for quantification.

IR imaging has also been extended recently to tissue imaging. A rhenium tris-carbonyl derivative **23c** incorporated into phospholipid micelles (bicosomes) was found to exhibit higher penetration into the skin than when dissolved in DMSO.<sup>48</sup> Monitoring by FTIR microspectroscopy showed that 40% of the rhenium derivatives reached the deeper epidermis when delivered via bicosomes, as compared to 5% via DMSO. This was clearly demonstrated with IR mapping of the treated skin using the  $A_1$  and E bands of the rhenium carbonyl. Policar

and co-workers have also developed a fluorescence and IR bimodal rhenium derivative conjugated to a nona-arginine peptide, **25**, for transdermal delivery into the skin (figure 7d).<sup>49</sup> The topical penetration of the conjugates, via the extracellular matrix, was determined by IR and fluorescence imaging of the skin slice. The conjugate was localized in the stratum corneum of the skin after 6 h of exposure, and deeper penetration into the epidermis was found after 24 h.

In the examples described thus far, which use a metal carbonyl as an exogenous probe in conventional 2D-IR imaging, the extraction of information at various depths is difficult owing to the complicated topography of the sample. More recently, the incorporation of tilt-series IR tomography with standard benchtop IR microscopy has allowed the acquisition of IR images at various coordinates. These can be reconstructed to generate 3D IR tomographic images, and was demonstrated with the use of  $[\text{Re}(\text{CO})_3(\text{H}_2\text{O})_3]^+$  in *Allium cepa* plant cells; the concentration of the Re complex was quantified (e.g., 10 mM in the cell nucleus) through accurate determination of the optical path from the reconstructed 3D images.<sup>50</sup>

#### 2.1.4 Photothermally induced resonance (PTIR) for subcellular IR imaging using AFM-IR microscope

A fundamental limitation on the use of IR spectroscopy for imaging lies with its spatial resolution, which is in the micrometer range. A technical breakthrough was the use of photothermally induced resonance (PTIR), reported by Policar, *et. al.*, for the subcellular IR imaging of a metal carbonyl (figure 8).<sup>51</sup> Localization of the  $[\text{CpRe}(\text{CO})_3]$ -hydroxytamoxifen analogue **24** in the cell nucleus of MDA-MB-231 cells was demonstrated. The technique, patented by Dazzi, *et. al.*, comprised an atomic force microscope (AFM) coupled with a tunable pulsed infrared laser. The working principle is based on the temperature rise in the sample accompanying absorption of the laser pulse. This increase in local temperature resulted in local thermal deformation, causing the AFM cantilever to oscillate with an amplitude that was correlated to the

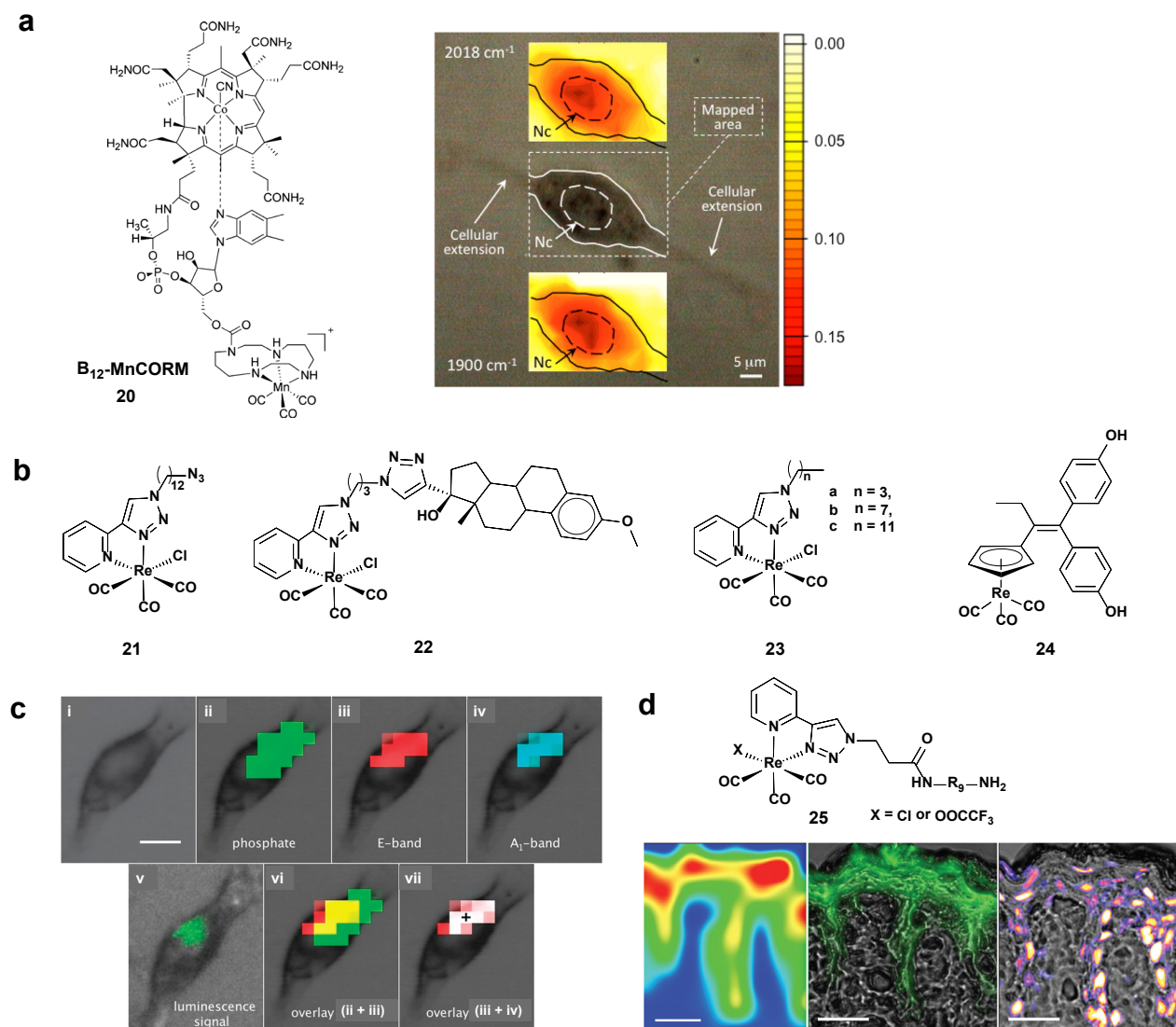


**Figure 7.** a) Molecular structure of the vitamin B<sub>12</sub>-Mn CORM conjugate **20** and optical images of a 3T3 fibroblast after incubation with **20** (1 mM). The top and bottom inserts show images reconstructed from integration of the intensity of the carbonyl stretching vibrations at 2018 and 1900 cm<sup>-1</sup>, respectively. The scale represents units of integrated band area in an absorbance vs wavenumber spectrum. Nc = cell nuclear area. Adapted from ref. 42 with permission from the American Chemical Society. b) Molecular structures of various rhenium derivatives used as IR and luminescent dual-modal probes. c) MDA-MB-231 cell incubated with **21** (10 μM, 1 h). (i) Bright field image (scale bar 10 μm). (ii–iv) SR-FTIR mappings, pixel size: 3 × 3 mm<sup>2</sup>: (ii) phosphate asymmetric stretching (green), (iii) E-band (red), (iv) A<sub>2</sub>-band (cyan). (v) Epifluorescence image, localization of **21** (green). (vi–vii) Overlays of SR-FTIR hot spots: (vi) overlay (yellow) of ii (green) and iii (red), (vii) overlay (white) of iii (red) and iv (cyan). Adapted from ref. 43 with permission from The Royal Society of Chemistry. d) Skin slice after a 24 h-exposure to a 2 × 10<sup>-2</sup> M solution of **25** in water. Left: mapping of the integral of the absorbance of the A<sub>1</sub>-band (2040–2000 cm<sup>-1</sup>). Middle: bright field image merged with the luminescence signal of **25**. Right: bright field image merged with the staining of nuclei by DAPI. Scale bar 20 μm. Reproduced from ref. 49 with permission from The Royal Society of Chemistry.

absorbance. The spatial resolution achievable corresponds to that of the AFM, i.e., 20–50 nm.

## 2.2 Metal carbonyls for chemical sensing

Besides the intensity for quantitation, the qualitative shift in frequency of the CO vibrations has also proven useful for sensing applications. The design of metal carbonyl “bioprobes” that give spectroscopic response upon interaction with the target was first discussed by Stephenson.<sup>52</sup> The term “bioprobes” refers to molecular structures that can provide information about biological systems. They are required to possess functions such as recognition, transduction and response.

### 2.2.1 pH sensing

Metal carbonyl π-complexes containing pH-sensitive groups like carboxylic acids and amines, can be used as pH-sensitive IR probes (figure 9).<sup>53</sup> Examples include η<sup>6</sup>-(1-carboxybenzene)Cr(CO)<sub>3</sub> (**26**) and η<sup>4</sup>-1-carboxy-1,3-pentadiene)Fe(CO)<sub>3</sub> (**27**). Protonation/deprotonation of these groups affect the ν<sub>sym</sub>(CO) and ν<sub>asym</sub>(CO) vibrational modes. Thus deprotonation of the carboxylic acid group increases the electron density of the π-conjugated system, thereby increasing π-back donation from the metal to C-O π\* anti-bonding orbital, which is translated into a shift to lower wavenumber of the CO vibrations.

The response to pH can also be tuned through the use of other pH-sensitive groups like hydroxyl or amine groups, or

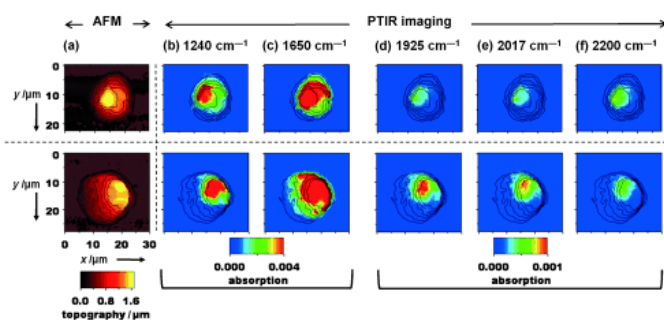


**Figure 8.** Images of MDA-MB-231 cells. Top row: control cells; bottom row: cells treated with a 10  $\mu\text{M}$  solution of **24** for 1 h at 37  $^{\circ}\text{C}$ . a) AFM topography; b–f) PTIR mappings at different wavelengths, with the AFM contours superimposed as black lines; the wavelengths correspond to the following bands: phosphate (b), amide (c), tricarbonyl (d and e), and out of band (f). Reproduced from ref. 51 with permission from John Wiley and Sons.

through different substitution on the  $\pi$ -system. A combination of two pH-active probes (**26** and **27**) with non-overlapping CO frequencies can act effectively as a “dual-sensor”. This allows simultaneous but independent measurements, increasing reliability, and since the probes have different  $\text{pK}_a$ 's (2.9 for **26** and 4.2 for **27**), they respond to different pH and hence allows a wider pH range that can be probed.

### 2.2.2 Metal cations sensing

The use of a benzo-15-crown-5- $\text{Cr}(\text{CO})_3$  complex **28** to sense alkali metal ions was first demonstrated by Creaser and Stephenson (figure 10a).<sup>54, 55</sup> Crown ethers have high affinity for alkali cations and hence, coupling them to metal carbonyl sensors allow the CO vibrations to act as readout signals via FT-IR spectroscopy. Complex **28** was found to be sensitive to  $\text{Na}^+$  and  $\text{K}^+$  ions, with concentration-dependent shifts of the symmetric and asymmetric stretches to higher wavenumbers; these are indicative of a reduction in the  $\pi$ -back donation from the metal. Binding of different  $\text{M}^+$  resulted in different electronic and structural changes to the two oxygen atoms bonded directly to the benzene ring. This induced different  $\sigma$  and  $\pi$  contributions to the Cr-CO bond and hence different frequency shifts. This is useful as most real analytes have more than one cation present. In an extended study, a principal components analysis (PCA) of the IR spectra for analytes with various compositions of cations ( $\text{Li}^+$ ,  $\text{Na}^+$  and  $\text{K}^+$ ), and  $\text{ClO}_4^-$  as the anion, in the 1890–1880  $\text{cm}^{-1}$  region was carried out to give a qualitative factor score plot.<sup>55</sup> The latter allows the qualitative difference in the spectra to be correlated to the different ratio of cations.

In another example, Moore and co-workers reported the use of (bipyridyl) $\text{Re}(\text{CO})_3$ , with an aza-15-crown-5-ether linked via an alkenyl or alkynyl-pyridine spacer to the metal center (**29–31**), as a cation sensor (figure 10b).<sup>56</sup> The CO vibrations showed, however, minimal shifts ( $\leq 1 \text{ cm}^{-1}$ ) as the crown ether was remote from the  $\text{Re}(\text{CO})_3$  moiety. Instead, shifts in the bond vibrations associated with the linker were more pronounced; to higher wavenumber for the  $\text{C}\equiv\text{C}$  vibration at  $\sim 2200 \text{ cm}^{-1}$ , and to lower wavenumber for the Ph-N vibration at  $\sim 1394 \text{ cm}^{-1}$ . These are because binding of a cation reduced the electron-donating effect of the nitrogen atom of the aza-

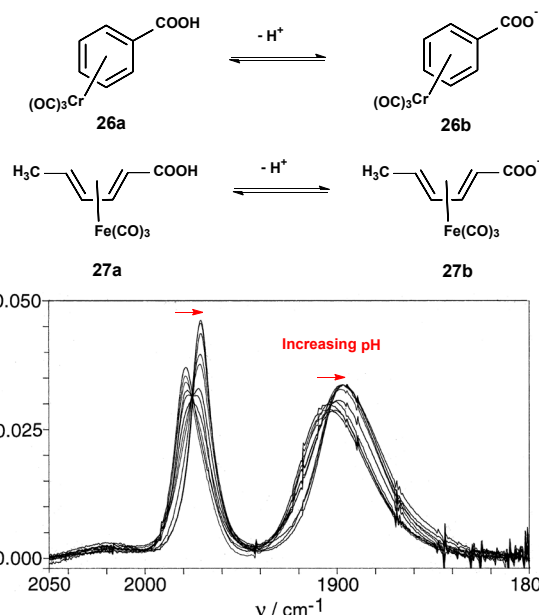


**Figure 9.** Molecular structures of **26** and **27** and their pH sensing capability. FTIR spectra in the 2050–1800  $\text{cm}^{-1}$  region of **26a** in buffer solutions over the pH range 2.1–6.0. Adapted from ref. 53 with permission from the American Chemical Society.

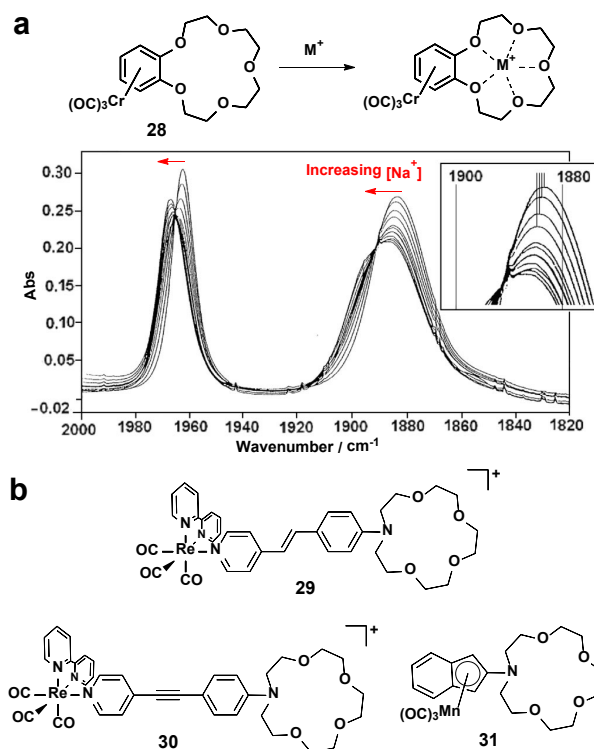


**Figure 10.** a) Interaction of metal ion with **28** and FTIR spectral overlay for **28-Na**<sup>+</sup>, with  $[\text{Na}^+]$  varying from 0 to 98 mM. Inset represents the expansion of the maxima observed for  $\nu_{\text{asym}}(\text{CO})$ . Adapted from ref. 55 with permission from John Wiley and Sons. b) Molecular structures of other metal carbonyl-crown ether conjugates for cation sensing.

crown-ether into the aromatic ring, thereby reducing the Ph-N but increasing the  $\text{C}\equiv\text{C}$  bond orders. The shifts were found to be more drastic with doubly charged cations like  $\text{Mg}^{2+}$ ,  $\text{Ca}^{2+}$  and  $\text{Ba}^{2+}$ , than with singly charged cations. The  $\eta^5\text{-Mn}(\text{CO})_3$ -indenyl crown ether conjugate **31** was similarly reported to complex with  $\text{Li}^+$  and  $\text{Na}^+$  ions to effect a modest shift of 2  $\text{cm}^{-1}$

1. Protonation at the nitrogen atom of the aza-crown ether can, on the other hand, effect a much greater shift in the CO vibrations (by as much as  $36\text{ cm}^{-1}$ ) and altering the basicity of the organometallic complex.

### 2.2.3 Anions sensing

Sensitive and selective sensing of carboxylate ions was achieved with  $\text{Cr}(\text{CO})_3$  conjugated to urea derivatives (figure 11a).<sup>57</sup> The  $\text{Cr}(\text{CO})_3$  group not only acts as an IR reporting group, but also enhanced its solubility in ethanol. Furthermore, it acted as an electron acceptor to turn the urea subunit into a good hydrogen-bond donor, thus improving their binding selectivity for carboxylates via N-H...O hydrogen bonding. Interestingly, high selectivity for carboxylate ions ( $\text{AcO}^-$ ) was achievable even in the presence of competitive protic solvents like ethanol. A control experiment involving **32** in acetonitrile showed that the addition of  $\text{AcO}^-$  led to  $\nu(\text{CO})$  shifts to higher wavenumbers which remained unchanged with the addition of ethanol. The sensitivity towards various concentration ranges of the carboxylate could also be tuned through the substituent on the urea moiety; while **32a** showed saturation at 6 mM, it was 14 mM for **32b**.

Fan and co-workers reported a series of stable  $\text{CpMn}(\text{CO})_2\text{L}$ , **33**, where L is hydroxypyridine or an N-heterocyclic ligand bearing an -OH or -NH moiety, for halide sensing (figure 11b).<sup>58</sup> The CO vibrations in these complexes shifted to lower wavenumber in the presence of various halides, and the shifts were correlated to the strength of the binding, i.e., in the order:  $\text{F}^- > \text{Cl}^- > \text{Br}^-$ . The OH...X<sup>-</sup> or NH...X<sup>-</sup> interactions (where X<sup>-</sup> refers to a halide) increased electron donation from the nitrogen atom to the metal center, thereby increasing  $\pi$ -back donation from metal to CO  $\pi^*$  orbital.

### 2.2.4 Hydrogen bond and $\pi$ -interaction sensing

$\pi$ -stacking interactions are ubiquitous in biological and chemical systems,<sup>59-62</sup> and are responsible for the stabilization of the double-helix in DNA and the tertiary structure of proteins.<sup>59, 60</sup> This interaction can also occur with aromatic cyclopentadienyl- (Cp) or arene-containing metal complexes. The first example which made use of this was IR sensing with  $(\eta^6\text{-arene})\text{-Cr}(\text{CO})_3$  complex, **34** (figure 12).<sup>63</sup> Addition of 1,3,5-trimethoxybenzene (TMB) or 1,2-dimethoxybenzene (DMB) to a cyclohexane solution of **34** resulted in the appearance of low wavenumber bands which have been attributed to  $\pi$ -stacking; this interaction increases the electron density on the arene ring of the complex, thereby enhancing  $\pi$ -back donation from the metal. Curve-fitting showed the presence of more than one set of these lower frequency bands and hence multiple stacking of the analytes. The complexes  $[\text{M}(\text{CO})_5(\text{L})]$  [L = (E)-1,2-di-4-pyridylethene; M = Cr (**35a**), W (**35b**)], which contain a free pyridine on one end of the ligand L, acted as hydrogen-donor sensors via the lone pair on the nitrogen;<sup>64</sup> hydrogen-donors like diphenylamine, 4-nitrophenyl(phenyl)amine and imidazole, were found to shift in the CO vibrations (mainly the E and  $A_{1ax}$  modes) to higher wavenumber. Shifts of up to  $20\text{ cm}^{-1}$  was observed, and they

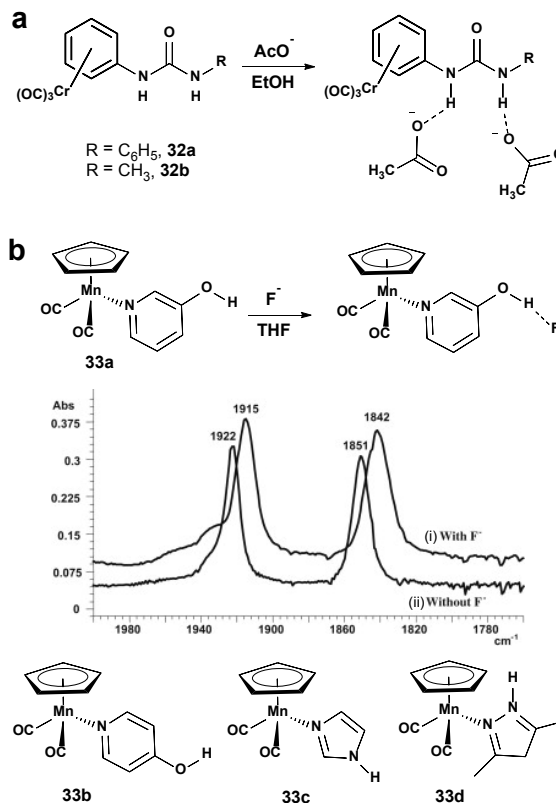


**Figure 11.** a) Interaction of urea- $\text{Cr}(\text{CO})_3$  conjugates, **32**, with acetate ions. b) FTIR spectra of the  $\nu_{\text{CO}}$  bands of  $\text{CpMn}(\text{CO})_2(3\text{-hydroxypyridine})$ , **33a**, (i) with 10 equivalents of  $\text{F}^-$  and (ii) without  $\text{F}^-$ , in THF. Molecular structures of  $\text{CpMn}(\text{CO})_2$  with N-heterocyclic ligands with an -OH or -NH moiety. Reproduced from ref. 57 with permission from Elsevier.

could be reversed by the introduction of a stronger hydrogen-bond acceptor like  $\text{O}=\text{PPh}_3$ .

### 2.2.5 Protein interaction sensing

A responsive metal carbonyl which gives a spectral change upon reaction with a functional group may be advantageous for reaction monitoring, especially in cases where excess probes are difficult to remove. The complex  $(\eta^4\text{-diene})\text{-Fe}(\text{CO})_3$ , **36**, which bears a labile pyridinium group, can generate the  $(\eta^5\text{-dienyl})\text{-Fe}(\text{CO})_3$  moiety which can then react readily with an amine functionality (figure 13).<sup>65</sup> Incubation of the protein  $\alpha$ -chymotrypsin with excess **36** led to the emergence of high frequency shoulders on the  $\nu_{\text{sym}}$  and  $\nu_{\text{asym}}$  stretches. Curve-fitting analysis resolved the spectrum of the bound complex from that of the excess **36**, and was identified to be that of the isolated species  $[\text{Fe}(\text{CO})_3(\text{C}_6\text{H}_7\text{NH}_2\text{Pr}^+)](\text{PF}_6)$ . The interaction of **36** with various amino acids and poly(lysine) also afforded species exhibiting similar spectra, and the study was extended to other enzymes like ribonuclease A, alkaline phosphatase and triacylglycerol lipase.<sup>66</sup> With a change in pH which results in deprotonation/protonation of the amine group, the spectrum of the enzyme-bound complex could undergo further shifts, thus demonstrating the dual-function of **36** as a tag and a pH sensor on the protein surface.

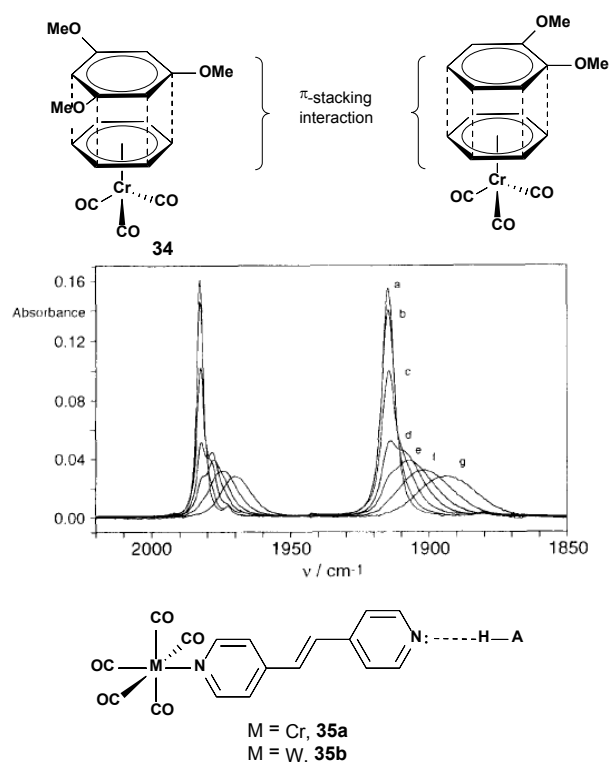


**Figure 12.** Top: Molecular structure of **34** and the  $\pi$ -stacking interaction with aromatic analytes. Middle: FTIR spectra of 0.45 mM **34** in cyclohexane (a), and in 39 mM (b), 79 mM (c), 392 mM (d), 785 mM (e), 1.57 M (f) and 3.92 M (g) solutions of 1,2-dimethoxybenzene in cyclohexane. Reproduced from ref. 63 with permission from Elsevier. Bottom: Molecular structure of **35** and the interaction with H-bond donor.

### 2.2.6 Solvent environment sensing

The observation of solvent-induced frequency shifts in metal carbonyls was made as early as in the 1960s by R. S. Nyholm and co-workers.<sup>67</sup> Typically, CO vibrational frequencies are shifted and broadened in the presence of polar solvents. Quantitative interpretation of the shifts was first carried out by Stephenson *et al.* using a series of ( $\eta^6$ -arene)-Cr(CO)<sub>3</sub> and ( $\eta^4$ -cyclohexadiene)-Fe(CO)<sub>3</sub> complexes, **37** (figure 13).<sup>68</sup>

Bellamy-type plots of  $\nu_{\text{sym}}$  against  $\nu_{\text{asym}}$  stretches of **37a** in various solvents were obtained and showed that the frequency shifts gave a better correlation with the solvent environment than the band broadening. The vibrational frequencies of **37a** in a binary solvent mixture of ethyl acetate and dimethyl acetamide showed good quantitative correlation with the composition, and the correlation for a ternary solvent mixture could be resolved with principal components analysis. Extension of the idea to metal carbonyl grafted onto a solid support for sensing binary to ternary solvent mixtures was demonstrated with ( $\eta^4$ -cyclohexadiene)-Fe(CO)<sub>2</sub>(L), where L = CO or PPh<sub>3</sub>, covalently attached onto silica particles via a 3-(diethoxymethylsilyl)propyl linker.<sup>69, 70</sup>

### 2.3 Ultrafast vibrational lifetime of metal carbonyls in proteins and membrane studies

The vibrational lifetime of metal carbonyls in organic solvents was first reported many years ago,<sup>71</sup> but it was only recently

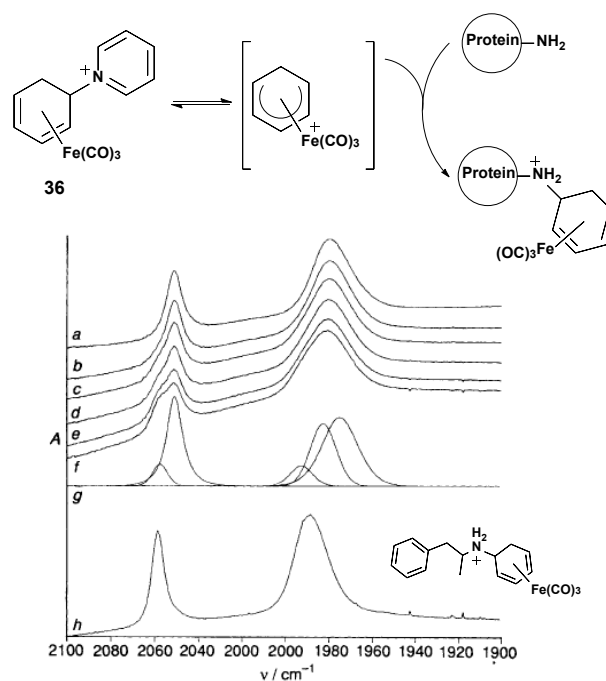


**Figure 13.** Top: Reaction of **36** with amine functionality in proteins. Bottom: (a-f) FTIR spectra of **36** in pH 7.5 buffer solution containing  $\alpha$ -chymotrypsin recorded at intervals over 3 h. (g) Component bands resulting from decomposition of spectrum c using a scale expansion of 2. (h) FTIR spectrum of [Fe(CO)<sub>3</sub>(C<sub>6</sub>H<sub>7</sub>NH<sub>2</sub>Pr)](PF<sub>6</sub>) in buffer. Adapted from ref. 65 with permission from The Royal Chemical Society.

that the vibrational lifetime in water was measured by Kurbaych and co-workers in their study on the water-soluble [RuCl<sub>2</sub>(CO)<sub>2</sub>]<sub>2</sub>, also known as CORM-2.<sup>72</sup> The vibrational relaxation was probed by two-dimensional (2D) IR spectroscopy, and showed that there was a big difference in the relaxation time in water ( $3.12 \pm 0.29$  ps) compared to that in a polar organic solvent like methanol ( $42.25 \pm 3$  ps).

This property was subsequently utilized in a study to probe the hydration environment at the protein-water interface (figure 15a).<sup>73</sup> The study employed metal carbonyls as a site-specific IR label on globular proteins, such as, hen egg white lysozyme (HEWL) and human lysozyme (HuLys). The proteins were labelled by incubating with tricarbonylchloro(glycinato)ruthenium(II) (CORM-3); while HEWL was labelled at the His15 residue to form [(His15)Ru(CO)<sub>2</sub>(H<sub>2</sub>O)<sub>3</sub>]<sup>2+</sup>, HuLys was labelled at the His78 residue.<sup>74</sup> Vibrational relaxation times of the ruthenium carbonyl residue measured in H<sub>2</sub>O, D<sub>2</sub>O, and in an amphiphilic alcohol cosolvent of D<sub>2</sub>O-trifluoroethanol to mimic a hydrophobic environment, suggested that the residue on HEWL experienced dynamically constrained water in a largely hydrophobic surface of the protein, while that on HuLys was more exposed and experienced bulk-like hydration dynamics.

The ruthenium carbonyl-labelled HEWL was also used to investigate hydration and protein dynamics using a glycerol/D<sub>2</sub>O mixture (figure 15a).<sup>75</sup> It was demonstrated that the bulk solvent had only a weak influence on the hydration water around the protein, and that there was strong coupling

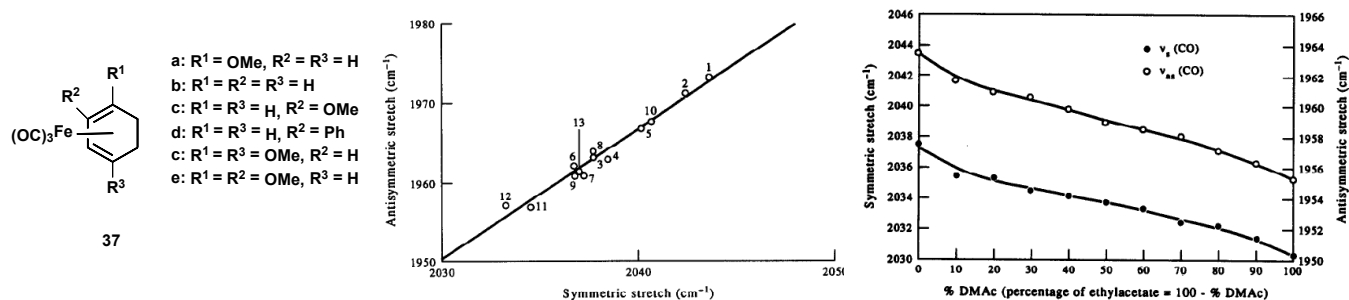


**Figure 14.** Left: Molecular structures of various  $(\eta^1\text{-cyclohexadiene})\text{-Fe}(\text{CO})_3$  complexes, **37**, used for solvent environment sensing. Middle: Symmetric and antisymmetric stretching frequencies of **37a** in various solvents: 1, hexane; 2, cyclohexane; 3, toluene; 4, dichloromethane; 5, diethyl ether; 6, tetrahydrofuran; 7, acetonitrile; 8, ethyl acetate; 9, acetone; 10, 1-octanol; 11, dimethyl formamide; 12, dimethyl acetamide; 13, acetic anhydride. Right: Variation of  $\nu_{\text{sym}}$  and  $\nu_{\text{asym}}$  of **37a** in binary mixtures of ethyl acetate and dimethyl acetamide. Reproduced from ref. 68 with permission from Elsevier.

between hydration and protein dynamics. In another study on the effects of crowding using macromolecular crowders like polyethylene glycol 400 (PEG400) and excess lysozymes, an abrupt hydration slowdown in the protein-hydration dynamics was observed when the concentration of crowders reached a threshold level; the macromolecular property of the crowders induced an “independent-to-collective hydration transition” in the protein.<sup>76</sup>

A similar dependence of the CO frequencies and lifetime on the solvent environment was also demonstrated with a series of  $\text{CpRe}(\text{CO})_3$  with linkers to methanethiosulfonate (**38**) to tag cysteine residues (figure 15b).<sup>77</sup> The  $\text{CpRe}(\text{CO})_3$  moiety was also bioconjugated to the ribosomal protein CTL9 through an alkynyl linkage (**39**) which was then coupled to an azidohomoalanine residue on the C-terminal domain of the protein via a “click” reaction (figure 15c).<sup>78</sup> The vibrational lifetimes of the metal carbonyl probe in  $\text{H}_2\text{O}$  and  $\text{D}_2\text{O}$  were found to be different, showing accessibility to the solvent.

The ultrafast vibrational dynamics of a metal carbonyl tagged to the active site of a *de novo* metalloenzyme from the TRI-family peptide was recently studied with two-dimensional infrared spectroscopy.<sup>79</sup> The homotrimer of parallel, coiled  $\alpha$ -helices contained a His3-Cu(I) metal site where CO was bound and acted as a vibrational probe. The ultrafast dynamics of the Cu-CO showed an unexpected non-equilibrium frequency shift with a 2 ps time scale. Computational modelling suggested that the electrostatic environment could be transduced via the histidine side chains to affect their binding orientation to the Cu center. This in turn mediated coupling between the CO stretch and the Cu-C-O bending motions, leading to the unprecedented observation.

The water-membrane interface in a model lipid membrane has also been probed with the introduction of a chromium tricarbonyl-labelled cholesterol, **40** (figure 15d).<sup>80</sup> The frequency-frequency correlation function (FFCF) at the water-membrane interface showed a distinct three-fold slowdown compared to that in bulk water. A similar incorporation of  $\text{W}(\text{CO})_6$  into the alkane interior of the membrane bilayer allowed sensing of its environment through the CO vibrations, and probing of the internal structural dynamics via 2D-IR measurements.<sup>81</sup> It was found that the addition of cholesterol induced a slowdown in the structural dynamics, and an abrupt

change occurred when the concentration reached 35%; this change was also observed in the FT-IR absorption spectra and ascribed to a phase change.

### 3. Applications in Raman spectroscopy

#### 3.1 IR vs Raman characteristics of CO

The inelastic scattering of a photon was first observed experimentally by C.V. Raman in 1928.<sup>82</sup> It involves a change in the polarizability of the molecule (with respect to the vibrational motion) induced by the oscillating electric field of the incident light. Light scattered from a molecule contains both elastic Rayleigh and inelastic Raman scattering. Rayleigh scattering corresponds to the scattering at the same frequency of the incident light, while Raman scattering involves a shift in the frequency of the incident light, which can be to a lower frequency (Stokes,  $\nu_o - \nu_j$ ) or to a higher frequency (anti-Stokes,  $\nu_o + \nu_j$ ); the shifts are associated with vibrational modes of the molecule (figure 16).<sup>83</sup> Rayleigh scattering is of much greater intensity than Raman scattering (a factor of  $\sim 10^6 - 10^8$ ) and by the Boltzmann distribution, more molecules will be in the vibrational ground state than the excited state at ambient conditions and hence, Stokes scattering is of higher intensity than anti-Stokes scattering. The Stokes scattering is what is usually recorded as the Raman shift with respect to the Rayleigh scattering. The difference between IR and Raman spectroscopy are summarized in table 1.

The intensity of a Raman signal is inherently weak, and its molecular determinant is termed the Raman cross-section ( $\beta$ ); it is analogous to molar extinction in absorption spectroscopy. In general,  $\beta$  is a function of the chemical bonds and other electronic factors.<sup>84</sup> For instance, molecules with extended  $\pi$  systems such as benzene, naphthalene and anthracene, in which the electrons are easily polarized, have large  $\beta$ . In contrast, small molecules without electron-rich atoms, like  $\text{H}_2$  and CO, have small  $\beta$  and hence produce weak Raman scattering. The CO ligand in a complex will likewise have a small Raman cross-section. For applications in biological systems,<sup>85-88</sup> Raman spectroscopy has two advantages over IR spectroscopy – the relatively weak Raman scattering of water, and sub-cellular resolution with simple instrumentation. The latter derives from the fact that the incident light for Raman

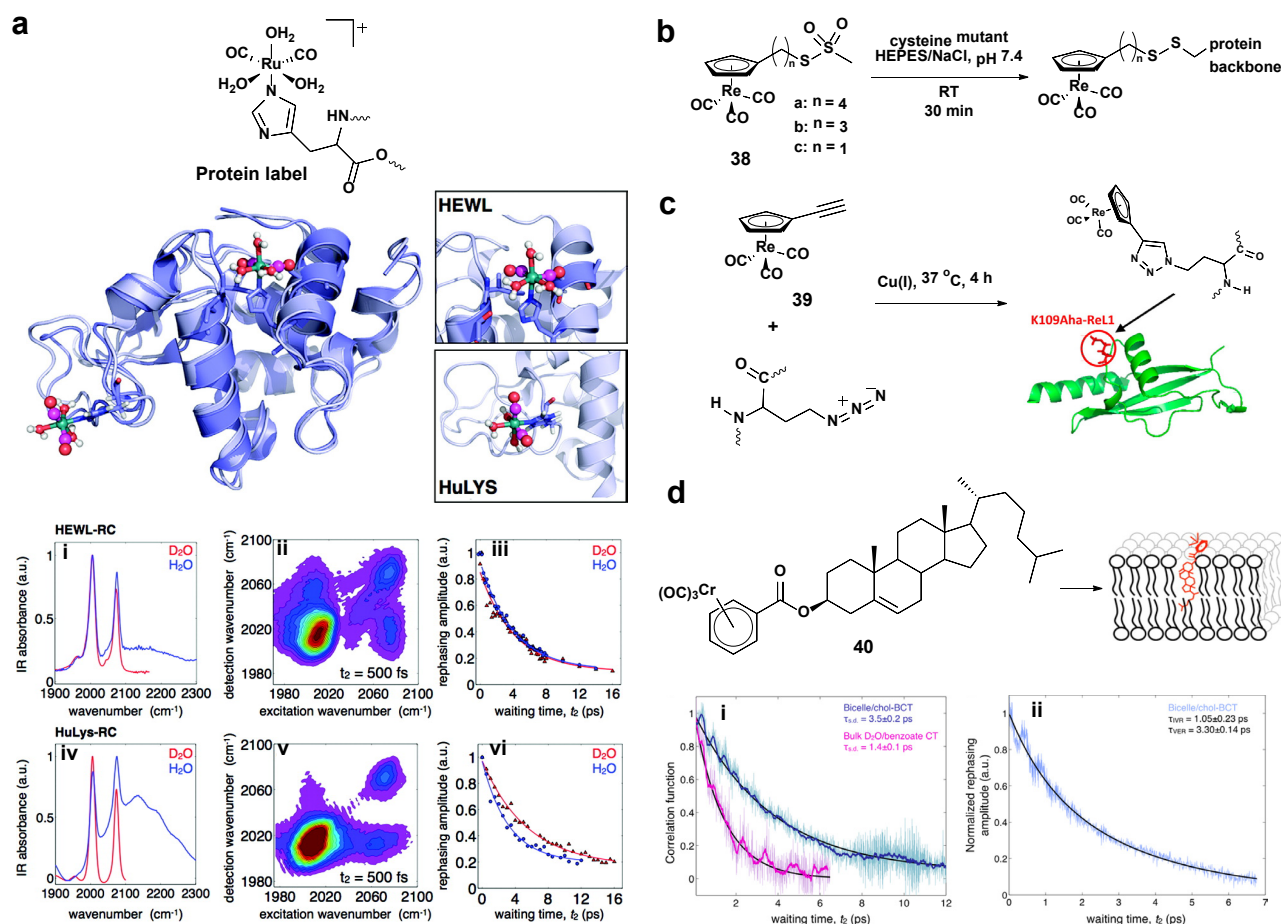


**Figure 15.** a) Molecular structure of ruthenium carbonyl (RC) protein label on HEWL and HuLYs. Crystal structures of HEWL-RC (PDB code 2XJW) overlaid with the crystal structure of native HuLYs (PDB code 2ZIJ). While no crystallographic data are available for the HuLYs-RC complex, the binding location is proposed by comparison with the HEWL-RC complex. Linear FTIR spectra of HEWL-RC (i) and HuLYs-RC (iv) in D<sub>2</sub>O and H<sub>2</sub>O. The 2D-IR rephasing spectra for HEWL-RC (ii) and HuLYs-RC (v) in D<sub>2</sub>O are shown for a waiting time of  $t_2 = 500$  fs. Monitoring the amplitude of the 2004 cm<sup>-1</sup> peak as a function of waiting time,  $t_2$ , provides the vibrational lifetime of the mode. For HEWL-RC there is no observable isotope effect in the vibrational relaxation between D<sub>2</sub>O and H<sub>2</sub>O (iii), whereas HuLYs-RC shows a very clear isotope effect (vi). Adapted from ref. 73 with permission from the American Chemical Society. b) Incorporation of CpRe(CO)<sub>3</sub> with an alkylated methanethiosulfonate onto thiol functionality on proteins. c) Bioorthogonal incorporation of a CpRe(CO)<sub>3</sub> alkyln derivative, **39**, onto residue 109 of the protein CTL9, located in a loop, using the “click” reaction. Adapted from ref. 78 with permission from the American Chemical Society. d) Incorporation of Cr(CO)<sub>3</sub> labelled cholesterol, **40**, into membrane constructs such as bicelles or unilamellar vesicles. i) Rapidly acquired spectral diffusion (RASD) measures the FFCF of **40** in bulk water and at the bicelle–water interface. The faint lines are the full data set; the thick colored lines are the result of a 100 fs windowed moving average. The fits are shown as black lines. ii) Rephasing decay for the bicelle sample showing the full data set (blue) and the biexponential fit. The sub-5-ps lifetime is indicative of water exposure. Adapted from ref. 80 with permission from the American Chemical Society.

**Table 1.** Summary and comparison between IR and Raman spectroscopy

	IR spectroscopy	Raman spectroscopy
<b>Excitation wavelength</b>	Mid-IR region from 2500 nm to 25000 nm (4000 to 400 cm <sup>-1</sup> )	Visible–near IR region from 532 to 1064 nm
<b>Nature of techniques</b>	Light absorption	Inelastic light scattering
<b>Mechanism</b>	Requires a dipole moment change	Requires a change in polarizability
<b>Spatial resolution at the diffraction limit</b>	~ 1.3 to 12.5 μM	~ 266 nm to 532 nm
<b>Limitations</b>	Low spatial resolution and prone to interference by water	Weak signals for CO vibrational frequencies.

excitation is in the visible to near-IR range and since spatial resolution scales as  $\sim \lambda/2$ , it provides nm as opposed to μm resolution for IR spectroscopy.

### 3.2 Metal carbonyls as probes for Raman imaging of cells

Despite the fundamental limitation of weak Raman scattering in metal carbonyls, compounded by the low concentration of the compound (in the μM range), the uptake of the manganese complex [Mn(tpm)(CO)<sub>3</sub>]Cl, **41**, in HT29 human colon cancer cells was studied with 3D Raman imaging and it was concluded that the complex was localized in the nuclear membrane and nucleolus (figure 17).<sup>89, 90</sup> In another example, a multi-modal Re(CO)<sub>3</sub>-mestranol derivative, **22**, was utilized as a probe for confocal Raman imaging of MDA-MB-231 cells; correlative imaging studies involving a series of luminescence and other vibrational techniques was also carried out.<sup>44</sup>

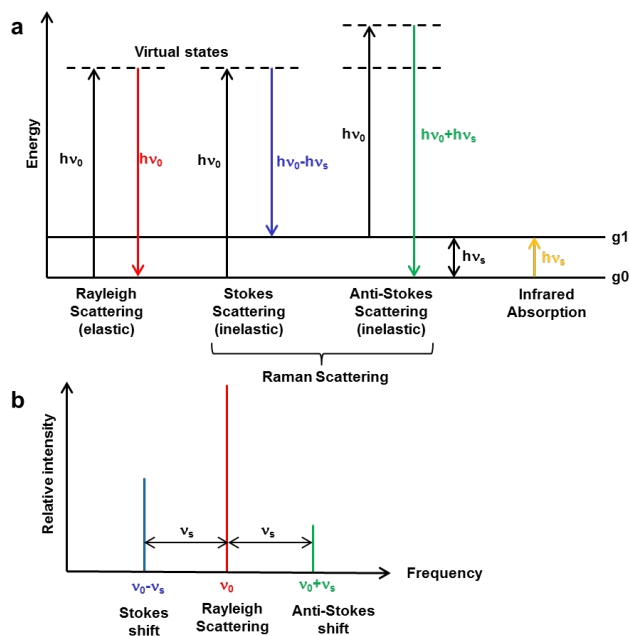


**Figure 16.** a) Jablonski diagram representing the energy transition for Rayleigh, Raman scattering and IR absorption. b) A schematic Raman spectrum showing the placement of the Stokes and anti-Stokes shift in relation to the Rayleigh line.

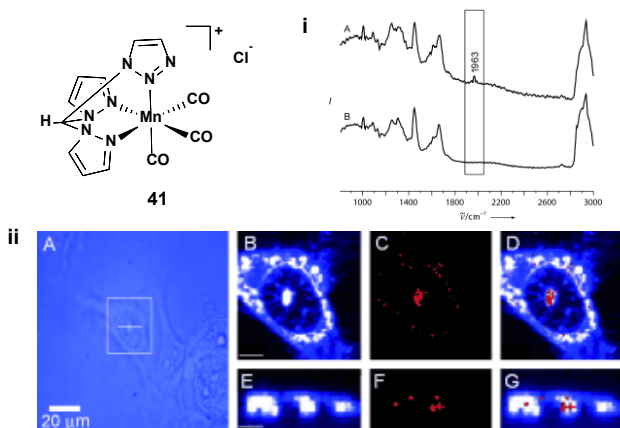


**Figure 17.** i) (A) Averaged Raman spectrum of the maximum signal of **41** inside a HT29 human colon cancer cell and (B) a typical averaged Raman spectrum from a region within the cell lacking any metal complex. ii) (A) Optical image of a HT29 human colon cancer cell incubated with an aqueous solution (2 mM) of **41** for 3 h. (B, C) Raman images reconstructed from integrating the intensities of the C-H and C=O stretching peaks. The integration range was  $2800\text{--}3050(\pm 2)\text{ cm}^{-1}$  for (B) and  $1945\text{--}1965(\pm 2)\text{ cm}^{-1}$  for (C). (D) Overlaid image of panels (B) and (C). (E-G) Cross-section Raman images along the x,z-direction of the same cell. Scanning positions are indicated by the white bar in the optical image. The scale bar for the Raman images is 6  $\mu\text{m}$ . Reproduced from ref. 89 with permission from John Wiley and Sons.

### 3.3 Detection through surface-enhanced Raman spectroscopy (SERS)

A paradigm shift occurred with the discovery of Raman intensity enhancement by Fleischmann and co-workers, and the subsequent investigation by Jeanmarie and Van Duyne.<sup>91, 92</sup> The phenomenon refers to the increase in the Raman intensity of a molecule on the surface of a metallic nanostructure; enhancement factors of  $10^6$  to  $10^9$  have been

reported. It led to the development of surface enhanced Raman scattering (SERS) and widespread applications followed.<sup>88, 93-96</sup> The mechanism of SERS has been studied over the last few decades,<sup>97-99</sup> and it is now widely accepted that the enhancement is the product of two mechanisms: electromagnetic and chemical enhancement. Electromagnetic enhancement refers to the enhancement of both the incident and scattered signals by the surface plasmon of the metallic surface; the surface plasmon is the collective electron cloud at the surface of the metallic nanostructure. Chemical enhancement refers to a metal-to-adsorbate charge-transfer that can occur with chemisorbed species.

Although SERS has long been recognized as a sensitive tool for detection, its use with metal carbonyls for biosensing has only emerged recently. The following sections highlight the transition from mid-IR to SERS biosensing and imaging in the application of metal carbonyls. SERS application requires the use of highly reproducible substrates to enhance the CO vibrations; two types of substrate are used - colloidal and planar substrates.

#### 3.3.1 SERS-based detection using colloidal substrate

SERS tags used in biological systems typically consists of Raman-active molecules that act as reporters adsorbed onto the surface of plasmon-resonant gold or silver nanoparticles protected with a coating, and bio-functionalized with targeting biomolecules.<sup>100</sup> Even though silver gives a stronger SERS enhancement than gold, the latter is preferred due to their better biocompatibility, size distribution and long-term stability.<sup>101, 102</sup>

A number of reviews on SERS tags that comprise organic molecules as reporters for *in-vivo* imaging have appeared,<sup>100, 103</sup> but the first report on the use of metal carbonyls as Raman reporters in a SERS tag for live cell imaging appeared in 2012; it comprised the triosmium carbonyl cluster  $\text{Os}_3(\mu\text{-H})_2(\text{CO})_{10}$ , **42**, conjugated onto gold nanoparticles.<sup>104</sup> This organometallic-nanoparticle (OM-NP) conjugate showed strong Raman signals in the CO vibration region ( $1800\text{--}2200\text{ cm}^{-1}$ ), with an enhancement factor estimated at  $\sim 15,000$ . The OM-NP conjugates were non-toxic, showed good aqueous dispersibility and stability, and could be easily functionalized with the desired biomolecule to give conjugate **43** for targeted delivery; in this case, they were biofunctionalized with an antibody against epidermal growth factor receptors (EGFR), which are over-expressed in oral squamous cell carcinoma (OSCC) (figure 18).

#### 3.3.2 SERS-based detection on planar substrate

SERS enhancement can also be achieved with planar substrates. While nanoparticles are susceptible to aggregation and hence require methods to stabilize them, planar substrates comprising patterned metallic surfaces immobilized onto a platform are chemically more stable and resistant to aggregation, and have been used in both *in-vivo* and *in-vitro* SERS biosensing.<sup>105, 106</sup> Some of the patterned metallic substrates that have been developed include sphere template films,<sup>107</sup> nanoparticle-anchored surfaces,<sup>108</sup> biomimetic

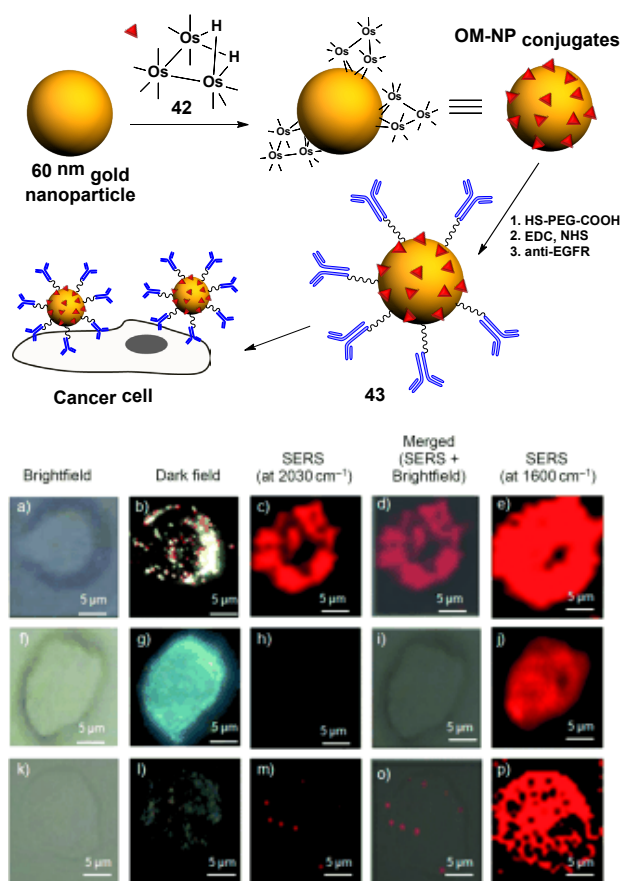


**Figure 18.** Preparation of OM-NP conjugates using the strong interactions of  $\text{Os}_3(\text{CO})_{10}(\mu\text{-H})_2$  (**42**) with gold nanoparticles. OM-NP conjugates are then functionalized with PEG and antibodies to give conjugate **43**. Bright-field, dark-field, and SERS mapping images of (a–e) OSCC cells, (f–j) SKOV cells treated with **43**, and (k–p) OSCC cells treated with anti-EGFR prior to incubation with **43**. All SERS mapping images of CO ( $2030\text{ cm}^{-1}$ ) and protein ( $1600\text{ cm}^{-1}$ ) were taken at an interval of  $1\text{ }\mu\text{m}$  ( $633\text{ nm}$  excitation). Reproduced from ref. 104 with permission from John Wiley and Sons.

substrates,<sup>109</sup> substrates with 3D Raman-active volume,<sup>110</sup> metallic film over nanospheres (MFON),<sup>106</sup> and bi-metallic film over nanospheres (BMFON).<sup>111</sup> Although differing in physical appearance and performance, all of these substrates serve to enhance the Raman signals of adsorbed molecules, with enhancement factors ranging from  $10^6$  to  $10^8$ .<sup>112</sup> The result is ultrasensitive detection, and they have been employed for the detection of a wide array of biological and chemical molecules,<sup>93, 112</sup> including viruses,<sup>113</sup> bacteria,<sup>114</sup> DNA,<sup>115</sup> glucose,<sup>116</sup> cancer biomarkers,<sup>117, 118</sup> explosives,<sup>119, 120</sup> transition metals,<sup>121</sup> and volatile organic compounds.<sup>122</sup> Many of these planar substrates allow direct detection of the target molecules, while others employ organic Raman reporters as labels. A problem with the latter is that many of them have signals that overlap with those of the cellular contents or of contaminants, making retrieval of the relevant information from the spectra difficult. For such cases, a metal carbonyl probe has proven useful.

The use of a triosmium carbonyl cluster-boronic acid conjugate, **44**, as a probe for the selective detection of glucose using Bimetallic Film Over Nanospheres (BMFON) as the SERS-active substrate was recently demonstrated in a sandwich

assay (figure 19).<sup>123</sup> The substrate was first functionalized with boronic acid which captures sugar molecules. Subsequent addition of **44** results in the selective labelling of glucose over fructose and galactose, as only the glucose molecule can bind to two boronic acid moieties simultaneously. Quantification through the CO stretching vibration of the conjugate was with a detection range of 0.1–10 mM. This glucose assay exhibited several advantages: (i) no prior purification of the sample was needed, (ii) an extremely low sample volume was tolerated, (iii) very high specificity for glucose, and (iv) good quantification as the spectroscopic signal was relatively free from interference by biomolecules.

Label-free detection, i.e., without the use of a labelling molecule, was demonstrated with a pH sensor comprising a  $\text{Cr}(\text{CO})_3$ -aminothiophenol functionalized BMFON substrate. This is the Raman analogue of the pH sensing via IR spectroscopy mentioned above, in which protonation of the  $-\text{NH}_2$  group leads to a shift in the CO vibrational frequency.<sup>53</sup> This sensor was tested with clinical urine samples and was able to differentiate between samples with pH 5.2 and 5.8 accurately.<sup>124</sup>

Label-free detection of alpha-1 antitrypsin (A1AT), a potential biomarker for bladder cancer,<sup>125</sup> was also demonstrated with a functional chip prepared by first depositing the triosmium carbonyl cluster  $\text{Os}_3(\text{CO})_{10}(\mu\text{-H})(\mu\text{-SCH}_2\text{CH}_2\text{COOH})$  onto BMFON, followed by the attachment of A1AT antibodies onto the carboxylic acid group (figure 19). Binding of A1AT with the antibodies induced changes in the CO vibrations which were concentration dependent but this had to be analyzed through principal component analysis (PCA). The potential for use in a clinical setting was verified with urine samples, which showed distinct demarcation in A1AT concentrations between normal and bladder cancer patients, with a detection range that covered the A1AT antigen levels in urine.

## 4. Summary and outlook

Transition metal carbonyl compounds are among the earliest known class of organometallic compounds and, for a very long time, the conventional wisdom has been that they are incompatible with biological systems. This started to change rapidly over the last 30 years, as this semi-chronological review has shown. The application of metal carbonyls in the biosciences which we have traced above, are based on three aspects of the vibrational spectroscopy of the CO ligand – intensity, frequency and lifetime: Intensity measurements allow for quantitation, essentially through Beer's law; frequency shifts are associated with chemical and physicochemical interactions and have led to chemical sensing applications; and vibrational lifetimes are a measure of the microenvironment and led to applications in proteins and membrane studies.

A shift to Raman spectroscopy offers some advantages: (a) it avoids the interference from water, which is of course ubiquitous in biological systems, and (b) it offers a better spatial resolution (in pure optical imaging), which is

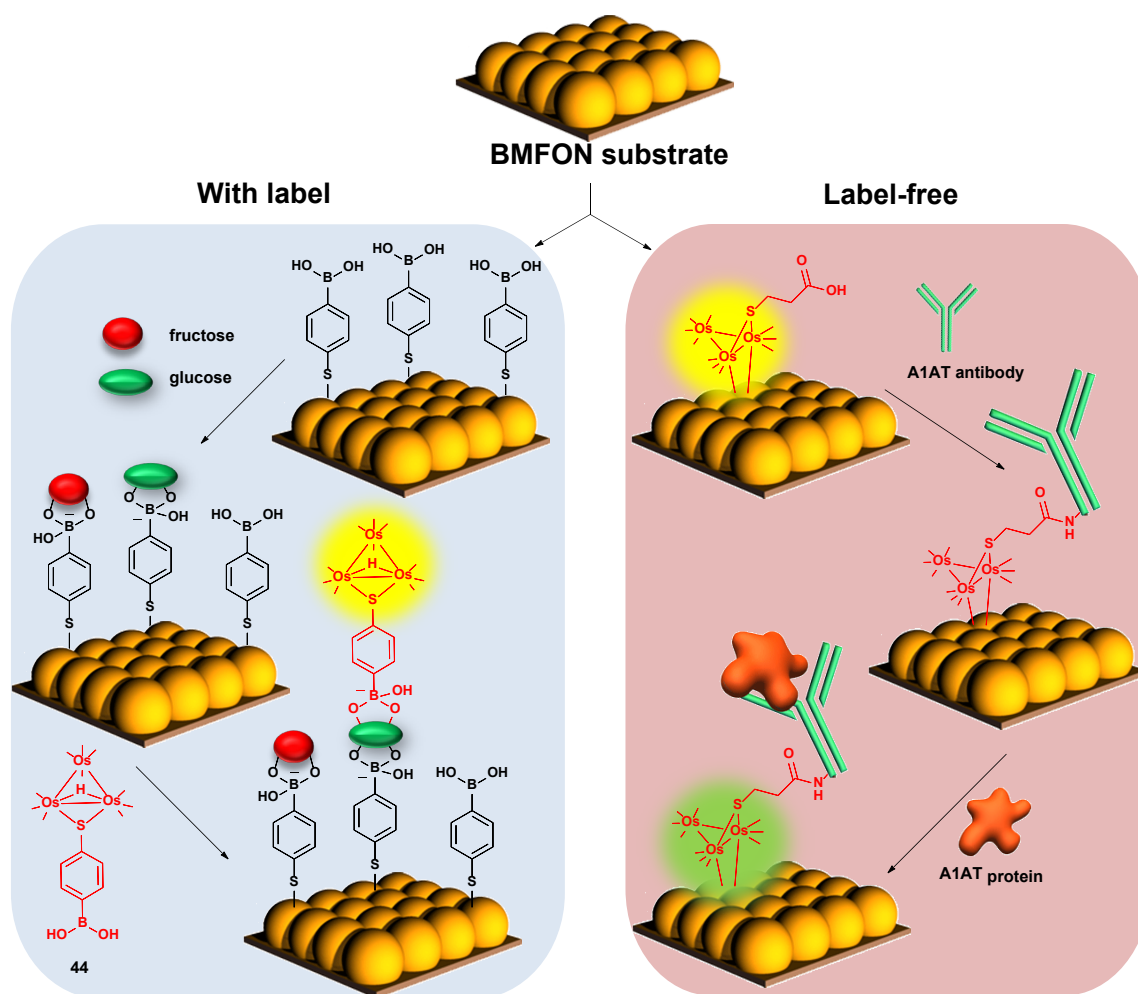


**Figure 19.** Schematic representation of the use of BMFON substrate with metal carbonyls for labelled and label-free SERS detection. Left: Carbohydrates were first anchored onto boronic acid-functionalized substrate, followed by selective detection of glucose using a trisium carbonyl cluster-boronic acid conjugate **44** as a spectroscopic label. Right: BMFON substrate was functionalized directly with  $\text{Os}_3(\text{CO})_{10}(\mu\text{-H})(\mu\text{-SCH}_2\text{CH}_2\text{COOH})$ , followed by conjugation to antibody. Spectral changes of the CO vibrational frequencies, induced by the addition of protein, can be detected and quantified by SERS. Adapted from ref. 125 with permission from John Wiley and Sons.

particularly important for subcellular work (although PTIR, which uses the AFM-IR setup, is able to achieve a high resolution of 20-50 nm with IR imaging (see section 2.1.4)). Applications based on direct detection by Raman spectroscopy are limited by the intrinsically weak Raman signals for CO vibrations. This can, however, be circumvented in many cases through SERS. A number of applications based on SERS enhancement have already emerged, and more are sure to come.

The further development of SERS-based applications will likely be connected to the need for reproducible SERS-active surfaces, and increasing and maintaining high enhancement factors. Strong enhancements can be obtained using substrates that contain “hot spots”; junctions between two or more closely-spaced gold or silver atoms. Extraordinary enhancements have been observed at junctions of multiple particles, compared to individual particles,<sup>126-128</sup> and examples include silver nanocluster arrays, gold nanoparticle dimers, trimers and nanoaggregates.<sup>129-131</sup> Reproducibility of the SERS substrate is a bottleneck, especially for translation to clinical use. Colloidal substrates are particularly prone to aggregation

as a result of the solvent and the presence of salts. Such random aggregation results in anomalous enhancements. It is therefore important to understand the interaction between the analytes and the nanostructures to achieve reproducibility; for metal carbonyls, little of this is known.

Translation of any of the applications to clinical use requires a number of issues to be resolved. These include reliability, portability, robustness, stability and cost-effectiveness, among others. As already alluded to above, reliability is currently probably a bigger issue for SERS-based applications than for those based on IR spectroscopy. Advances in instrumentation, such as the development of portable or hand-held spectrometers, will be important for portability. The other issues are related to the chemistry of the metal carbonyls, and cheaper alternatives for these (as well as for SERS substrates).

While the development of metal carbonyls in vibrational spectroscopy remains promising, there are limitations to the types of applications that are accessible by these techniques. For example, conventional IR spectroscopy is likely to be confined to applications on cellular or tissue surfaces as

interference by the large amounts of water in deep tissue is likely to impede their use for *in-vivo* applications. On the other hand, Raman or SERS imaging are generally limited to subcutaneous detection of SERS-encoded nanoparticles injected subcutaneously or accumulated near the surface (up to 5 mm depth) with the use of near-IR light source.<sup>132-134</sup> Recent advances in Raman techniques such as surface enhanced spatially offset Raman spectroscopy (SESORS) can, however, allow detection at a depth of 20-50 mm in tissue,<sup>135</sup> and 3-8 mm in bone.<sup>136</sup> These can potentially pave the way for the *in-vivo* application of metal carbonyls.

Nevertheless, the applications which have been described in this review are already wide-ranging, and they are only small samplings of huge classes in applications – imaging and sensing, of biomarkers, biologically important and other molecules, and microenvironments. More examples are sure to emerge with much that will be relevant to a clinical setting.

## Acknowledgements

We acknowledge the support from Nanyang Technological University and the Singapore Bioimaging Consortium, Agency for Science, Technology, and Research, Singapore (SBIC, A\*STAR). Z. L. was supported by an A\*STAR graduate scholarship.

## References

- 1 F. E. Paulik and J. F. Roth, *Chem. Commun.*, 1968, 1578a-1578a.
- 2 G. J. Sunley and D. J. Watson, *Catal. Today*, 2000, **58**, 293-307.
- 3 G. Natta and I. Pasquon, in *Advances in Catalysis*, eds. P. W. S. D.D. Eley and B. W. Paul, Academic Press, 1959, vol. Volume 11, pp. 1-66.
- 4 S. Top, G. Jaouen, A. Vessieres, J. P. Abjean, D. Davoust, C. A. Rodger, B. G. Sayer and M. J. McGlinchey, *Organometallics*, 1985, **4**, 2143-2150.
- 5 G. Jaouen and A. Vessieres, *Pure Appl. Chem.*, 1985, **57**, 1865-1874.
- 6 L. Mond, C. Langer and F. Quincke, *J. Chem. Soc., Trans.*, 1890, **57**, 749-753.
- 7 K. V. Kong, W. Chew, L. H. K. Lim, W. Y. Fan and W. K. Leong, *Bioconjugate Chem.*, 2007, **18**, 1370-1374.
- 8 G. Jaouen, *Bioorganometallics: Biomolecules, Labeling, Medicine*, Wiley-VCH Verlag GmbH & Co. KGaA, Weinheim, Germany, 2006.
- 9 G. Jaouen and M. Salmain, *Bioorganometallic Chemistry: Applications in Drug Discovery Biocatalysis, and Imaging*, Wiley-VCH Verlag GmbH & Co. KGaA, Weinheim, Germany, 2014.
- 10 I. S. Butler, R. P. Kengne-Momo, G. Jaouen, C. Policar and A. Vessières, *Appl. Spectrosc. Rev.*, 2012, **47**, 531-549.
- 11 A. Vessières, *J. Organomet. Chem.*, 2013, **734**, 3-16.
- 12 E. Licandro, M. Panigati, M. Salmain and A. Vessières, in *Bioorganometallic Chemistry*, eds. G. Jaouen and M. Salmain, Wiley-VCH Verlag GmbH & Co. KGaA, Weinheim, Germany, 2014, pp. 339-392.
- 13 L. Quaroni and F. Zobi, in *Inorganic Chemical Biology: Principles, Techniques and Applications*, ed. G. Gasser, John Wiley & Sons, Ltd, Chichester, UK, 2014, pp. 149-182.
- 14 S. Clède and C. Policar, *Chem. - Eur. J.*, 2015, **21**, 942-958.
- 15 G. Jaouen, A. Vessières, S. Top, A. A. Ismail and I. S. Butler, *J. Am. Chem. Soc.*, 1985, **107**, 4778-4780.
- 16 G. Jaouen, A. Vessieres, S. Top, M. Savignac, A. A. Ismail and I. S. Butler, *Organometallics*, 1987, **6**, 1985-1987.
- 17 A. Vessieres, G. Jaouen, M. Gruselle, J. L. Rossignol, M. Savignac, S. Top and S. Greenfield, *J. Steroid Biochem.*, 1988, **30**, 301-305.
- 18 S. Tondou, S. Top, A. Vessieres and G. Jaouen, *J. Chem. Soc., Chem. Commun.*, 1985, 326-328.
- 19 A. Vessieres, S. Tondou, G. Jaouen, S. Top, A. A. Ismail, G. Teutsch and M. Moguilewsky, *Inorg. Chem.*, 1988, **27**, 1850-1852.
- 20 M. Salmain, A. Vessières, P. Brossier, I. S. Butler and G. Jaouen, *J. Immunol. Methods*, 1992, **148**, 65-75.
- 21 A. A. Ismail, G. Jaouen, P. Cheret and P. Brossier, *Clin. Biochem.*, 1989, **22**, 297-299.
- 22 M. Salmain, A. Vessieres, I. S. Butler and G. Jaouen, *Bioconjugate Chem.*, 1991, **2**, 13-15.
- 23 A. Vessières, K. Kowalski, J. Zakrzewski, A. Stepien, M. Grabowski and G. Jaouen, *Bioconjugate Chem.*, 1999, **10**, 379-385.
- 24 V. Philomin, A. Vessières and G. Jaouen, *J. Immunol. Methods*, 1994, **171**, 201-210.
- 25 A. Vessières, N. Fischer-Durand, F. Le Bideau, P. Janvier, J.-M. Heldt, S. Ben Rejeb and G. Jaouen, *Appl. Organomet. Chem.*, 2002, **16**, 669-674.
- 26 N. Fischer-Durand, A. Vessières, J.-M. Heldt, F. le Bideau and G. Jaouen, *J. Organomet. Chem.*, 2003, **668**, 59-66.
- 27 M. Salmain, A. Vessieres, P. Brossier and G. Jaouen, *Anal. Biochem.*, 1993, **208**, 117-120.
- 28 M. Salmain, A. Vessières, A. Varenne, P. Brossier and G. Jaouen, *J. Organomet. Chem.*, 1999, **589**, 92-97.
- 29 M. Salmain, N. Fischer-Durand, L. Cavalier, B. Rudolf, J. Zakrzewski and G. Jaouen, *Bioconjugate Chem.*, 2002, **13**, 693-698.
- 30 N. Fischer-Durand, M. Salmain, B. Rudolf, A. Vessières, J. Zakrzewski and G. Jaouen, *ChemBioChem*, 2004, **5**, 519-525.
- 31 N. Fischer-Durand, M. Salmain, B. Rudolf, L. Dai, L. Jugé, V. Guérineau, O. Laprèvote, A. Vessières and G. Jaouen, *Anal. Biochem.*, 2010, **407**, 211-219.
- 32 C.-M. Yam, C.-M. Pradier, M. Salmain, N. Fischer-Durand and G. Jaouen, *J. Colloid Interface Sci.*, 2002, **245**, 204-207.
- 33 C.-M. Pradier, M. Salmain, L. Zheng and G. Jaouen, *Surf. Sci.*, 2002, **502-503**, 193-202.
- 34 C.-M. Yam, L. Zheng, M. Salmain, C.-M. Pradier, P. Marcus and G. Jaouen, *Colloids Surf., B*, 2001, **21**, 317-327.
- 35 B. Rudolf, M. Salmain, J. Grobelny, G. Celichowski and E. Tomaszewska, *Colloids Surf., A*, 2011, **385**, 241-248.
- 36 B. Rudolf, M. Salmain, J. Grobelny, G. Celichowski and M. Cichowski, *J. Organomet. Chem.*, 2013, **734**, 32-37.

- 37 B. Rudolf, M. Salmay, A. Z. Wilczewska, A. Kubicka, I. Misztalewska and N. Fischer-Durand, *Colloids Surf., A*, 2014, **457**, 142-151.
- 38 C. C. Romão and H. L. A. Vieira, in *Advances in Organometallic Chemistry and Catalysis*, ed. A. J. L. Pombeiro, John Wiley & Sons, Inc., 2013, pp. 543-561.
- 39 U. Schatzschneider, *Br. J. Pharmacol.*, 2015, **172**, 1638-1650.
- 40 U. Schatzschneider, *Inorg. Chim. Acta*, 2011, **374**, 19-23.
- 41 I. Chakraborty, S. J. Carrington and P. K. Mascharak, *Acc. Chem. Res.*, 2014, **47**, 2603-2611.
- 42 F. Zobi, L. Quaroni, G. Santoro, T. Zlateva, O. Blacque, B. Sarafimov, M. C. Schaub and A. Y. Bogdanova, *J. Med. Chem.*, 2013, **56**, 6719-6731.
- 43 S. Clède, F. Lambert, C. Sandt, Z. Gueroui, M. Refregiers, M.-A. Plamont, P. Dumas, A. Vessières and C. Policar, *Chem. Commun.*, 2012, **48**, 7729-7731.
- 44 S. Clède, F. Lambert, C. Sandt, S. Kascakova, M. Unger, E. Harte, M.-A. Plamont, R. Saint-Fort, A. Deniset-Besseau, Z. Gueroui, C. Hirschmugl, S. Lecomte, A. Dazzi, A. Vessières and C. Policar, *Analyst*, 2013, **138**, 5627-5638.
- 45 S. Clède, F. Lambert, R. Saint-Fort, M.-A. Plamont, H. Bertrand, A. Vessières and C. Policar, *Chem. - Eur. J.*, 2014, **20**, 8714-8722.
- 46 S. Clède, F. Lambert, C. Sandt, Z. Gueroui, N. Delsuc, P. Dumas, A. Vessières and C. Policar, *Biotechnol. Adv.*, 2013, **31**, 393-395.
- 47 I. Kitanovic, S. Can, H. Alborzina, A. Kitanovic, V. Pierroz, A. Leonidova, A. Pinto, B. Spingler, S. Ferrari, R. Molteni, A. Steffen, N. Metzler-Nolte, S. Wölfl and G. Gasser, *Chem. - Eur. J.*, 2014, **20**, 2496-2507.
- 48 E. Fernández, G. Rodríguez, S. Hostachy, S. Clède, M. Cócera, C. Sandt, F. Lambert, A. de la Maza, C. Policar and O. López, *Colloids Surf., B*, 2015, **131**, 102-107.
- 49 S. Clède, N. Delsuc, C. Laugel, F. Lambert, C. Sandt, A. Baillet-Guffroy and C. Policar, *Chem. Commun.*, 2015, **51**, 2687-2689.
- 50 L. Quaroni, M. Obst, M. Nowak and F. Zobi, *Angew. Chem. Int. Ed.*, 2015, **54**, 318-322.
- 51 C. Policar, J. B. Waern, M.-A. Plamont, S. Clède, C. Mayet, R. Prazeres, J.-M. Ortega, A. Vessières and A. Dazzi, *Angew. Chem. Int. Ed.*, 2011, **50**, 860-864.
- 52 G. R. Stephenson, in *Bioorganometallics*, ed. G. Jaouen, Wiley-VCH Verlag GmbH & Co. KGaA, 2006, pp. 215-262.
- 53 C. E. Anson, T. J. Baldwin, C. S. Creaser, M. A. Fey and G. R. Stephenson, *Organometallics*, 1996, **15**, 1451-1456.
- 54 C. E. Anson, C. S. Creaser and G. R. Stephenson, *J. Chem. Soc., Chem. Commun.*, 1994, 2175-2176.
- 55 G. R. Stephenson, C. E. Anson, C. S. Creaser and C. A. Daul, *Eur. J. Inorg. Chem.*, 2011, **2011**, 2086-2097.
- 56 J. D. Lewis and J. N. Moore, *PCCP*, 2004, **6**, 4595-4606.
- 57 X. Tian, L. Song, Y. Yuan and J. Lin, *Organometallics*, 2010, **29**, 509-511.
- 58 J. W. Kee and W. Y. Fan, *J. Organomet. Chem.*, 2013, **729**, 14-19.
- 59 W. Saenger, *Principles of Nucleic Acid Structure*, Springer-Verlag, Berlin, 1984.
- 60 S. Burley and G. Petsko, *Science*, 1985, **229**, 23-28.
- 61 E. A. Meyer, R. K. Castellano and F. Diederich, *Angew. Chem. Int. Ed.*, 2003, **42**, 1210-1250.
- 62 C. A. Hunter and J. K. M. Sanders, *J. Am. Chem. Soc.*, 1990, **112**, 5525-5534.
- 63 C. E. Anson, C. S. Creaser and G. Richard Stephenson, *Spectrochim. Acta, Part A*, 1996, **52**, 1183-1191.
- 64 E. Peris, J. A. Mata and V. Moliner, *J. Chem. Soc., Dalton Trans.*, 1999, 3893-3898.
- 65 C. E. Anson, C. S. Creaser, O. Egedy, M. A. Fey and G. R. Stephenson, *J. Chem. Soc., Chem. Commun.*, 1994, 39-40.
- 66 C. E. Anson, C. S. Creaser, O. Egedy and G. R. Stephenson, *Spectrochim. Acta, Part A*, 1997, **53**, 1867-1877.
- 67 C. C. Barraclough, J. Lewis and R. S. Nyholm, *J. Chem. Soc.*, 1961, 2582.
- 68 C. S. Creaser, M. A. Fey and G. R. Stephenson, *Spectrochim. Acta, Part A*, 1994, **50**, 1295-1299.
- 69 C. S. Creaser, W. E. Hutchinson and R. G. Stephenson, *Appl. Spectrosc.*, 2000, **54**, 1624-1628.
- 70 C. S. Creaser, W. E. Hutchinson and G. R. Stephenson, *Analyst*, 2001, **126**, 647-651.
- 71 E. J. Heilweil, R. R. Cavanagh and J. C. Stephenson, *Chem. Phys. Lett.*, 1987, **134**, 181-188.
- 72 J. T. King, M. R. Ross and K. J. Kubarych, *J. Phys. Chem. B*, 2012, **116**, 3754-3759.
- 73 J. T. King, E. J. Arthur, C. L. Brooks and K. J. Kubarych, *J. Phys. Chem. B*, 2012, **116**, 5604-5611.
- 74 T. Santos-Silva, A. Mukhopadhyay, J. D. Seixas, G. J. L. Bernardes, C. C. Romão and M. J. Romão, *J. Am. Chem. Soc.*, 2011, **133**, 1192-1195.
- 75 J. T. King and K. J. Kubarych, *J. Am. Chem. Soc.*, 2012, **134**, 18705-18712.
- 76 J. T. King, E. J. Arthur, C. L. Brooks and K. J. Kubarych, *J. Am. Chem. Soc.*, 2014, **136**, 188-194.
- 77 A. M. Woys, S. S. Mukherjee, D. R. Skoff, S. D. Moran and M. T. Zanni, *J. Phys. Chem. B*, 2013, **117**, 5009-5018.
- 78 I. Peran, T. Oudenhoven, A. M. Woys, M. D. Watson, T. O. Zhang, I. Carrico, M. T. Zanni and D. P. Raleigh, *J. Phys. Chem. B*, 2014, **118**, 7946-7953.
- 79 M. R. Ross, A. M. White, F. Yu, J. T. King, V. L. Pecoraro and K. J. Kubarych, *J. Am. Chem. Soc.*, 2015, **137**, 10164-10176.
- 80 D. G. Osborne, J. A. Dunbar, J. G. Lapping, A. M. White and K. J. Kubarych, *J. Phys. Chem. B*, 2013, **117**, 15407-15414.
- 81 O. Kel, A. Tamimi, M. C. Thielges and M. D. Fayer, *J. Am. Chem. Soc.*, 2013, **135**, 11063-11074.
- 82 C. V. Raman and K. S. Krishnan, *Nature*, 1928, **122**, 169.
- 83 L. A. Nafie, in *Handbook of Raman Spectroscopy*, eds. I. R. Lewis and H. G. M. Edwards, CRC Press, Boca Raton, FL, USA, 2001.
- 84 R. L. McCreery, in *Raman Spectroscopy for Chemical Analysis*, John Wiley & Sons, Inc., Hoboken, NJ, USA, 2005, pp. 15-33.
- 85 T. W. Collette and T. L. Williams, *J. Environ. Monit.*, 2002, **4**, 27-34.
- 86 H. Yamakoshi, K. Dodo, A. Palonpon, J. Ando, K. Fujita, S. Kawata and M. Sodeoka, *J. Am. Chem. Soc.*, 2012, **134**, 20681-20689.

- 87 K. Klein, Alexander M. Gigler, T. Aschenbrenner, R. Monetti, W. Bunk, F. Jamitzky, G. Morfill, Robert W. Stark and J. Schlegel, *Biophys. J.*, 2012, **102**, 360-368.
- 88 Q. Tu and C. Chang, *Nanomedicine: NBM*, 2012, **8**, 545-558.
- 89 K. Meister, J. Niesel, U. Schatzschneider, N. Metzler-Nolte, D. A. Schmidt and M. Havenith, *Angew. Chem. Int. Ed.*, 2010, **49**, 3310-3312.
- 90 P. Hildebrandt, *Angew. Chem. Int. Ed.*, 2010, **49**, 4540-4541.
- 91 M. Fleischmann, P. J. Hendra and A. J. McQuillan, *Chem. Phys. Lett.*, 1974, **26**, 163-166.
- 92 D. L. Jeanmaire and R. P. Van Duyne, *J. Electroanal. Chem.*, 1977, **84**, 1-20.
- 93 B. Sharma, R. R. Frontiera, A. I. Henry, E. Ringe and R. P. Van Duyne, *Mater. Today*, 2012, **15**, 16-25.
- 94 W. Xie and S. Schlucker, *PCCP*, 2013, **15**, 5329-5344.
- 95 K. Kneipp, H. Kneipp, I. Itzkan, R. R. Dasari and M. S. Feld, *Chem. Rev.*, 1999, **99**, 2957-2976.
- 96 K. Saha, S. S. Agasti, C. Kim, X. Li and V. M. Rotello, *Chem. Rev.*, 2012, **112**, 2739-2779.
- 97 A. Campion and P. Kambhampati, *Chem. Soc. Rev.*, 1998, **27**, 241-250.
- 98 P. L. Stiles, J. A. Dieringer, N. C. Shah and R. P. Van Duyne, *Annu. Rev. Anal. Chem.*, 2008, **1**, 601-626.
- 99 M. Moskovits, *PCCP*, 2013, **15**, 5301-5311.
- 100 Y. Wang, B. Yan and L. Chen, *Chem. Rev.*, 2012, **113**, 1391-1428.
- 101 S. Lee, H. Chon, M. Lee, J. Choo, S. Y. Shin, Y. H. Lee, I. J. Rhyu, S. W. Son and C. H. Oh, *Biosens. Bioelectron.*, 2009, **24**, 2260-2263.
- 102 S. Abalde-Cela, P. Aldeanueva-Potel, C. Mateo-Mateo, L. Rodríguez-Lorenzo, R. A. Alvarez-Puebla and L. M. Liz-Marzán, *J. R. Soc., Interface*, 2010, **7**, S435-S450.
- 103 K. K. Maiti, U. S. Dinish, A. Samanta, M. Vendrell, K.-S. Soh, S.-J. Park, M. Olivo and Y.-T. Chang, *Nano Today*, 2012, **7**, 85-93.
- 104 K. V. Kong, Z. Lam, W. D. Goh, W. K. Leong and M. Olivo, *Angew. Chem. Int. Ed.*, 2012, **51**, 9796-9799.
- 105 J. M. Yuen, N. C. Shah, J. T. Walsh, M. R. Glucksberg and R. P. Van Duyne, *Anal. Chem.*, 2010, **82**, 8382-8385.
- 106 D. A. Stuart, C. R. Yonzon, X. Zhang, O. Lyandres, N. C. Shah, M. R. Glucksberg, J. T. Walsh and R. P. Van Duyne, *Anal. Chem.*, 2005, **77**, 4013-4019.
- 107 X. Zhang, A. V. Whitney, J. Zhao, E. M. Hicks and R. P. Van Duyne, *J. Nanosci. Nanotechnol.*, 2006, **6**, 1920-1934.
- 108 K. C. Grabar, K. J. Allison, B. E. Baker, R. M. Bright, K. R. Brown, R. G. Freeman, A. P. Fox, C. D. Keating, M. D. Musick and M. J. Natan, *Langmuir*, 1996, **12**, 2353-2361.
- 109 N. L. Garrett, P. Vukusic, F. Ogrin, E. Sirotkin, C. P. Winlove and J. Moger, *J. Biophotonics*, 2009, **2**, 157-166.
- 110 K. A. Stoerzinger, J. Y. Lin and T. W. Odom, *Chem. Sci.*, 2011, **2**, 1435-1439.
- 111 C. Y. Fu, K. W. Kho, U. S. Dinish, Z. Y. Koh and O. Malini, *J. Raman Spectrosc.*, 2012, **43**, 977-985.
- 112 R. A. Tripp, R. A. Dluhy and Y. Zhao, *Nano Today*, 2008, **3**, 31-37.
- 113 S. Shanmukh, L. Jones, J. Driskell, Y. Zhao, R. Dluhy and R. A. Tripp, *Nano Lett.*, 2006, **6**, 2630-2636.
- 114 W. R. Premasiri, D. T. Moir, M. S. Klempner, N. Krieger, G. Jones and L. D. Ziegler, *J. Phys. Chem. B*, 2005, **109**, 312-320.
- 115 Y. Wen, W. Wang, Z. Zhang, L. Xu, H. Du, X. Zhang and Y. Song, *Nanoscale*, 2013, **5**, 523-526.
- 116 K. E. Shafer-Peltier, C. L. Haynes, M. R. Glucksberg and R. P. Van Duyne, *J. Am. Chem. Soc.*, 2003, **125**, 588-593.
- 117 L. Guerrini, E. Pazos, C. Penas, M. E. Vázquez, J. L. Mascareñas and R. A. Alvarez-Puebla, *J. Am. Chem. Soc.*, 2013, **135**, 10314-10317.
- 118 M. Li, S. K. Cushing, J. Zhang, S. Suri, R. Evans, W. P. Petros, L. F. Gibson, D. Ma, Y. Liu and N. Wu, *ACS Nano*, 2013, **7**, 4967-4976.
- 119 D. A. Stuart, K. B. Biggs and R. P. Van Duyne, *Analyst*, 2006, **131**, 568-572.
- 120 J. M. Sylvia, J. A. Janni, J. D. Klein and K. M. Spencer, *Anal. Chem.*, 2000, **72**, 5834-5840.
- 121 K. Kim, J. W. Lee and K. S. Shin, *Analyst*, 2013, **138**, 2988-2994.
- 122 K. Kim, J. W. Lee, D. Shin, J.-Y. Choi and K. S. Shin, *Analyst*, 2012, **137**, 1930-1936.
- 123 K. V. Kong, Z. Lam, W. K. O. Lau, W. K. Leong and M. Olivo, *J. Am. Chem. Soc.*, 2013, **135**, 18028-18031.
- 124 K. V. Kong, U. S. Dinish, W. K. O. Lau and M. Olivo, *Biosens. Bioelectron.*, 2014, **54**, 135-140.
- 125 K. V. Kong, W. K. Leong, Z. Lam, T. Gong, D. Goh, W. K. O. Lau and M. Olivo, *Small*, 2014, **10**, 5030-5034.
- 126 E. C. Le Ru, E. Blackie, M. Meyer and P. G. Etchegoin, *J. Phys. Chem. C*, 2007, **111**, 13794-13803.
- 127 Z. Wang, S. Pan, T. D. Krauss, H. Du and L. J. Rothberg, *Proc. Natl. Acad. Sci. U. S. A.*, 2003, **100**, 8638-8643.
- 128 P. H. C. Camargo, M. Rycenga, L. Au and Y. Xia, *Angew. Chem. Int. Ed.*, 2009, **48**, 2180-2184.
- 129 W. J. Cho, Y. Kim and J. K. Kim, *ACS Nano*, 2012, **6**, 249-255.
- 130 G. Chen, Y. Wang, M. Yang, J. Xu, S. J. Goh, M. Pan and H. Chen, *J. Am. Chem. Soc.*, 2010, **132**, 3644-3645.
- 131 P.-J. Huang, L.-K. Chau, T.-S. Yang, L.-L. Tay and T.-T. Lin, *Adv. Funct. Mater.*, 2009, **19**, 242-248.
- 132 S. Keren, C. Zavaleta, Z. Cheng, A. de la Zerda, O. Gheysens and S. S. Gambhir, *Proc. Natl. Acad. Sci. USA*, 2008, **105**, 5844-5849.
- 133 C. L. Zavaleta, B. R. Smith, I. Walton, W. Doering, G. Davis, B. Shojaei, M. J. Natan and S. S. Gambhir, *Proc. Natl. Acad. Sci. USA*, 2009, **106**, 13511-13516.
- 134 X. Qian, X.-H. Peng, D. O. Ansari, Q. Yin-Goen, G. Z. Chen, D. M. Shin, L. Yang, A. N. Young, M. D. Wang and S. Nie, *Nat. Biotechnol.*, 2008, **26**, 83-90.
- 135 N. Stone, M. Kerssens, G. R. Lloyd, K. Faulds, D. Graham and P. Matousek, *Chem. Sci.*, 2011, **2**, 776-780.
- 136 B. Sharma, K. Ma, M. R. Glucksberg and R. P. Van Duyne, *J. Am. Chem. Soc.*, 2013, **135**, 17290-17293.